STUDY OF OPTICALLY PUMPED NH_3 MID-INFRARED LASERS

BY

CLAUDE ROLLAND, B.Sc.

A Thesis

Submitted to the School of Graduate Studies

in Partial Fulfillment of the Requirements

for the Degree

Master of Science

McMaster University

October 1980

MASTER OF SCIENCE (1980) McMASTER UNIVERSITY
(Physics) Hamilton, Ontario

TITLE: Study of Optically Pumped NH_3 Mid-Infrared Lasers

AUTHOR: Claude Rolland, B.Sc. (Université de Montréal)

SUPERVISORS: Professor B.K. Garside, Professor J. Reid

NUMBER OF PAGES: xiii, 82

ABSTRACT

The work described in this thesis concerns the investigation of the fundamental mechanism involved in off-resonant low power pumped NH_3 mid-infrared lasers. Our theoretical model shows two different contributions to the mid-infrared gain: a Raman-type term and an inversion term. Even if both gain contributions can be present in a laser medium, one process usually dominates over the other. These two processes are characterized by very different properties with respect to the lasing frequency, the magnitude of the gain and the pump absorption. Strong experimental evidence, based on the measurements of these various characteristics, has demonstrated that the Raman-type two quantum transition was responsible for lasing in the NH_3 lasers investigated.

One consequence of Raman lasing is the possibility of obtaining pumped MIR lasers with very low pumping powers. We report here pulsed threshold powers as low as 20 Watts peak which represents an improvement by a factor of 100 over the lowest MIR threshold previously reported. Furthermore, the main parameter influencing the pump threshold value, the offset between the pump frequency and the NH_3 absorption line center, was varied during our experiment. It is shown that a decrease of this pump offset frequency generally reduces the

pump threshold, but a very close pump coincidence produces the opposite effect. Consequently, we have estimated that the optimum pump offset for minimum pump power threshold is $\sim$ 100 MHz, for NH_3 in the 12 μm region (at room temperature).

One important extension of this work concerns the possibility of developing an optically pumped cw MIR laser. The low pump power thresholds and long MIR pulse lengths ($\sim$ 500 μsec) observed during this work indicate that cw MIR lasing is feasible.

ACKNOWLEDGEMENTS

I wish to express my deep appreciation to my supervisors Dr. B.K. Garside and Dr. J. Reid, for their guidance and support throughout this work.

I would like to thank my colleague T.A. Znotins for his precious help during the writing of this thesis. Thanks are also due to my colleague C. Dang for providing the laser diode measurements.

This work was supported by the Natural Sciences and Engineering Research Council Canada.

TABLE OF CONTENTS

FIGURE CAPTIONS

CHAPTER I

INTRODUCTION

In 1970, T. Y. Chang and T. J. Bridges reported the first optically pumped far infrared (FIR) laser [1]. This discovery came at a time when laser sources in the FIR region were almost nonexistent. The optical pumping technique uses powerful infrared (IR) lasers, such as carbon-dioxide, hydrogen-fluoride or deuterium-fluoride, to excite a particular vibrational mode in a molecular gas. The principal advantage of optical pumping over other excitation schemes (e.g. electrical discharge), is that it permits the selective excitation of a specific molecular transition without appreciably disturbing other molecular levels. Although such a scheme requires a pump frequency closely matched to the absorbing transition of the pumped molecule, the large collection of available FIR lines in the 30 μm to 2 mm range proves that the optical pumping technique is extremely well suited to generate coherent millimeter and submillimeter wave emissions [2,3]. Such long wavelengths correspond to purely rotational transitions. Figure 1 shows a molecular energy level diagram, with typical level populations corresponding to a molecule being optically pumped.

In 1976, the first vibrational-rotational inversion with respect to a ground vibrational state using optical

Fig. 1

Typical energy level structure of an optically pumped molecule. In one case, the ground state is pumped and FIR lasing occurs between two rotational levels ($J' \rightarrow J''$) within the same excited vibrational state. In the MIR case, the emission is a vibrational-rotational transition ($J' \rightarrow J''$ (MIR)). Also shown are typical thermal populations relative to a pumped level population of 100.

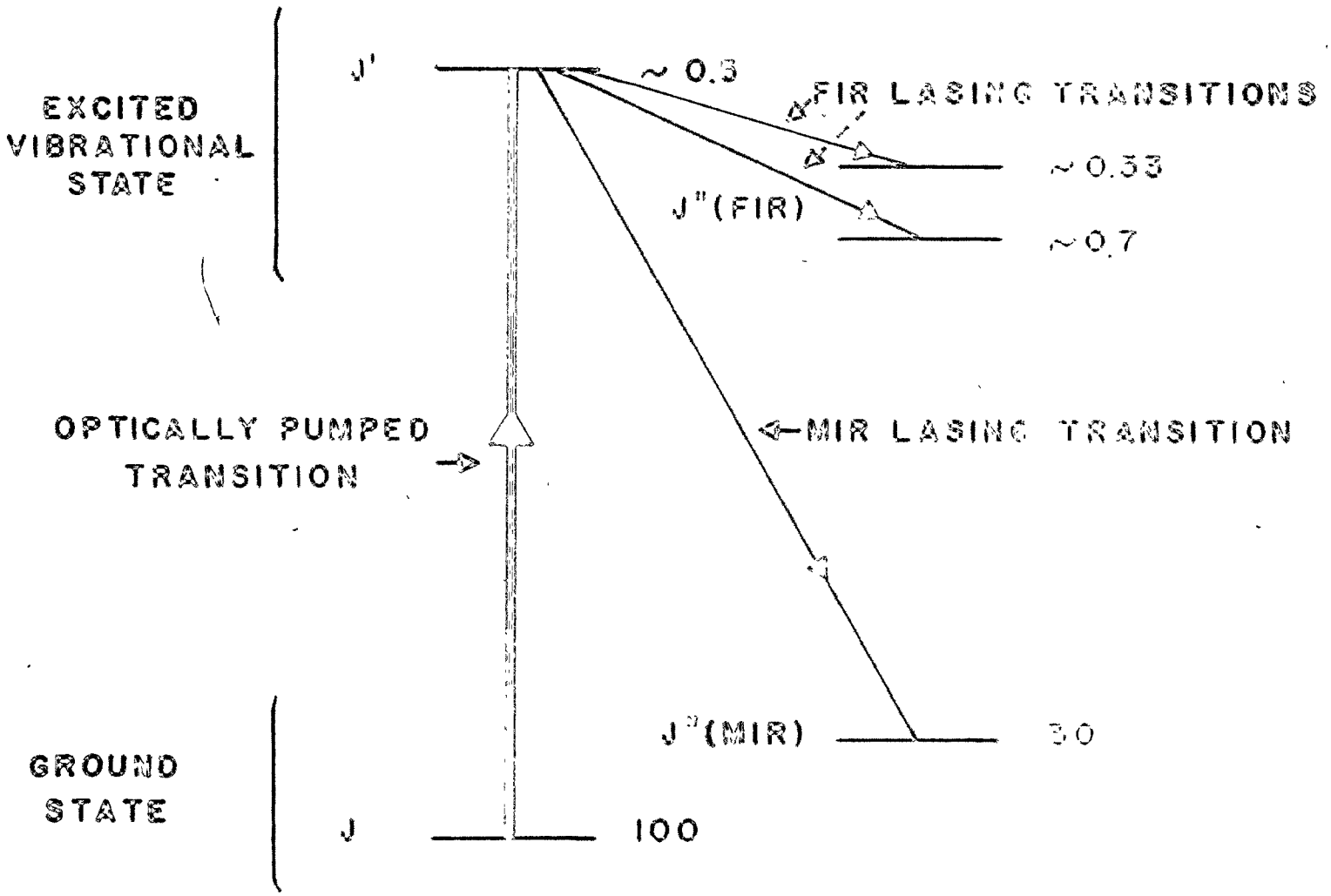
EXCITED VIBRATIONAL STATE
J'
~ 0.3
FIR LASING TRANSITIONS
~ 0.33
J"(FIR)
~ 0.7
OPTICALLY PUMPED TRANSITION
MIR LASING TRANSITION
J"(MIR)
30
GROUND STATE
J
100

pumping, was reported by T.Y. Chang and J.D. McGee [4]. The spectral range of these lasers lies in the mid-infrared region (MIR) i.e. between 10 μm and 30 μm which is typical of vibrational-rotational transitions (see Fig. 1). The potential utilization of these lasers in the fields of laser photochemistry [5] or laser isotope separation [6], has motivated many researchers to direct their work toward the development of efficient, high power optically pumped pulsed MIR lasers. However very little work has been done on investigating the possibility of developing optically pumped continuous (cw) MIR lasers. The main difficulty encountered in the development of such lasers relates to the small energy difference between the pumped level and the lower laser level which results in a high thermal population in the lower laser level. Consequently, due to the relatively low pumping power available from most cw sources, population inversion using a cw source has never been reported in the MIR region.

Recently, T.Y. Chang and J.D. McGee proposed an alternate mechanism to explain the operation of several off-resonant optically pumped pulsed MIR lasers [7]. This mechanism involves a Raman-type two quantum transition. A double quantum transition occurs when a molecule, generally in the ground state, undergoes a coherent transition to the lower level of the MIR transition by simultaneously absorbing a pump photon and emitting a MIR photon [8]. Such a process can create gain even

in the absence of population inversion. This fact turns out to be of crucial importance when we consider the possibility of low pumping powers, as would be required for the development of optically pumped cw MIR lasers. Furthermore, a clear understanding of the Raman process would provide valuable information regarding the laser dynamics of optically pumped pulsed MIR lasers.

This thesis constitutes the first attempt at investigating optically pumped MIR lasers at low pumping powers. The understanding of the fundamental process involved in such lasers is necessary for future developments toward an optically pumped cw MIR laser. The work described in this thesis is aimed at demonstrating the Raman nature of several low power pumped MIR lasers. In particular, it is known that the pump offset frequency (i.e. the difference between the line center of the absorbing transition and the pump frequency) constitutes a very important parameter in the Raman gain expression (as will be discussed in Chapter II). Consequently, we have chosen to investigate three different NH_3 transitions, covering a pump offset frequency range from 10 MHz to 1.4 GHz. The ammonia molecule was selected as the MIR laser medium for two major reasons: (i) the large number of NH_3 lasing transitions in the MIR region, (ii) the readily available and well known technology of the pump lasers (CO_2 and N_2O).

In this work, we have succeeded in substantially decreasing the NH_3 threshold pumping power from the usual hundreds

of kilowatts to power levels as low as 20 watts. The present work will thus study optically pumped MIR lasers at low levels of pumping power as are available in commercial cw pump lasers. Hence, the conclusions drawn from this thesis will be particularly pertinent for research oriented toward the development of cw MIR lasers.

This thesis is divided into six chapters. The theoretical considerations are outlined in Chapter II. This chapter includes a brief description of the ammonia molecule and of the particular NH_3 transitions studied. A simple theoretical model of the gain in optically pumped lasers is discussed, with emphasis on the major differences between the Raman and inversion processes. Considering our requirements for low pumping power, we designed a MIR cavity somewhat different from the ones conventionally employed. This cavity is described in Chapter III, along with the rest of the experimental apparatus. In Chapter IV, we begin our investigations of the NH_3 transitions. This is done by measuring the small signal absorption of the pump radiation as a function of the NH_3 pressure. Comparison between theory and our experiment confirms previously calculated [9] and observed [10,11] values for parameters such as pump offset frequencies, linestrengths and linewidths of the pumped transitions. These results are subsequently used in Chapter V where experimental evidence demonstrates the Raman nature of two NH_3 lasing

transitions studied. In contrast, despite the close coincidence between the pump frequency and the line center absorption of the third transition investigated (offset $\sim$ 10 MHz), lasing was not observed at our pumping levels. The significance of this result will be discussed in Chapter V. Finally, Chapter VI summarizes the consequences of the results presented in the previous chapters and from them we predict an optimum offset frequency which would minimize the pump threshold power.

CHAPTER II

THEORY

II.1 Introduction

This chapter gives a brief review of the NH_3 molecular structure and its energy level diagram. Emphasis is given to the three particular transitions that were involved in our investigation. A relatively simple theoretical model for an optically pumped MIR laser is proposed using the density matrix formalism. Several assumptions are made in deriving this model and the limitations imposed by these assumptions are discussed. Finally, an expression for the MIR gain is derived and its physical significance is examined. To this end, we present preliminary calculations which show the influence of the level populations on the gain behaviour.

II.2 NH_3 molecular structure

The NH_3 molecule has a symmetrical pyramidal structure, with a permanent dipole moment. The three hydrogen atoms are situated at the corners of a regular triangle. The nitrogen atom lies above (or below) the hydrogen plane and forms the top of a pyramid. The height of the ammonia pyramid is determined to be $.381\times10^{-8}$ cm and the H-H distance $r_o(H\text{-}H) = 1.628\times10^{-8}$ cm [12]. The point group corresponding to the ammonia molecule is C_{3v}. This implies the existence

of four fundamental modes, two totally symmetric modes (A_1) ν_1, ν_2 and two doubly degenerate modes (E) ν_3, ν_4 [13].

II.3 Energy diagram and selection rules

The NH_3 molecule has been extensively studied by spectroscopists over the years because of the intensity and richness of its spectrum. The multitude of transitions in the NH_3 spectrum is partly caused by the existence of both right and left handed forms [13]. These states are produced by the reflection of the nitrogen atom with respect to the hydrogen plane. The transformation of one form into the other occurs when the nitrogen atom is translated through the hydrogen plane (acting as a potential hill).

Each energy level of the pyramidal structure would be at least doubly degenerate if the potential barrier between the two states was infinitely high. In reality, a slight splitting appears in each vibro-rotational level due to the tunneling effect, as predicted by the quantum theory. In most pyramidal molecules the splitting is negligible or unresolved†. However, the energy separations between the inversion doubled levels in ammonia are exceptionally large. For example, in the $\nu_2 = 1$ fundamental mode, the size of the splitting is $\Delta\nu \sim 35.7\ cm^{-1}$ and increases with the vibrational quantum number. The four fundamental modes, ν_1, ν_2, ν_3, ν_4 and their respective inversion doubling are shown in Fig. 2 [13,14].

†For example, AsH_3 would take two years to go through a cycle of inversions and thus has no observable splitting [12].

Fig. 2

Energy levels of the lower vibrational modes in NH_3. The values of the corresponding inversion doubling are also given.

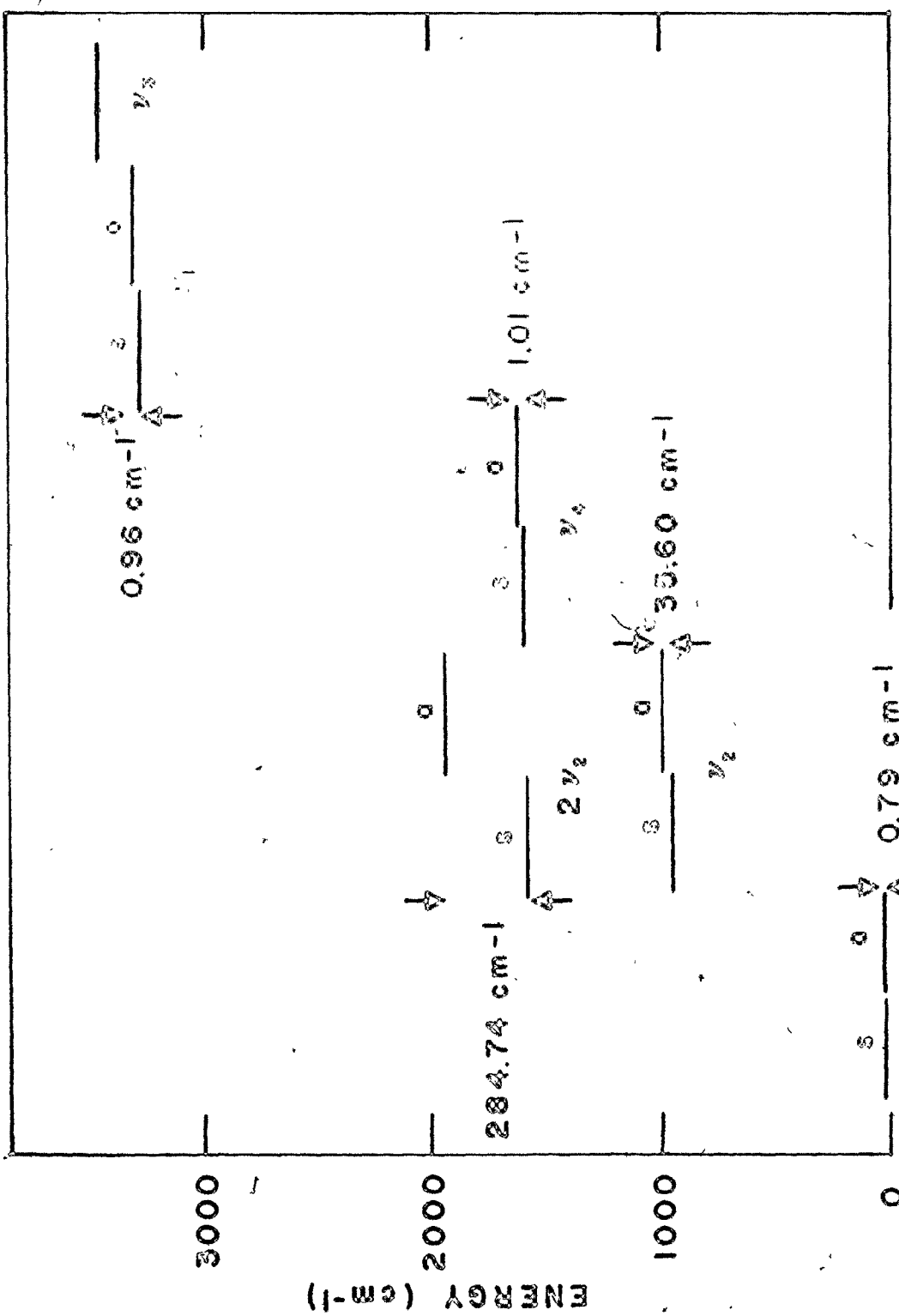
ENERGY (cm-1)
3000
2000
1000
0
GROUND STATE
0.79 cm-1
33.60 cm-1
1.01 cm-1
0.96 cm-1
284.74 cm-1
2 ν2
ν2
ν3
0
1
2
3

The two forms are labelled symmetric (s) and antisymmetric (a).

Two rotational quantum numbers, J and K, characterise each NH_3 rotational level. J corresponds to the total angular momentum, which has a (2J+1) degeneracy associated with the various possible orientations of J in space (M = J, J-1, ...,-J). K represents the projection of J on the NH_3 axis of symmetry. the quantum number K cannot be greater than J i.e. J = K, K+1,.... Each vibro-rotational transition is written as: $\alpha\beta(J,K)$ where β can be P, Q or R, corresponding to a change in J of $\Delta J = -1,0,1$ respectively, and α is either s or a. α, J and K always refer to the lower level of the transition.

The selection rules for vibrational-rotational electric dipole transitions in the infrared spectrum are [13]

$$\Delta K = 0 \qquad \Delta J = 0, \pm 1.$$

In addition, we have the symmetry selection rules

$$a \longleftrightarrow s \quad a \not\longleftrightarrow a \qquad s \not\longleftrightarrow s \quad ,$$

where $\longleftrightarrow$ and $\not\longleftrightarrow$ mean allowed and not allowed respectively. The selection rules for the Raman transitions differ from the IR ones. In the Raman case we have

$$K = 0 \qquad J = 0, \pm 1, \pm 2$$

$$a \not\longleftrightarrow s \qquad a \longleftrightarrow a \quad s \longleftrightarrow s$$

with the restriction $\Delta J = \pm 1$ does not apply when K = 0.

II.4 Laser transitions

In 1965, NH_3 laser action in pulsed electrical discharges was observed by Mathias *et al* [15]. Seven laser lines between 21 μm and 32 μm were identified. Since then, many additional laser lines have been discovered by optically pumping NH_3 with continuous or pulsed lasers [2,3]. Most of these laser transitions involve the $\nu_2 = 1$ state, as the upper laser level.

Lasing transitions can be divided into two categories: pure rotational transitions and vibrational-rotational transitions. As stated in Chapter I, we are particularly interested in vibro-rotational transitions i.e. transitions occuring in the 10-30 μm spectral range. Here, we chose to investigate three specific NH_3 lines. The relevant energy levels and transitions are shown in Fig. 3. The frequency offset between the pump frequency and the NH_3 line center absorption was the main criterion in the selection of these three lines. The pump frequency offsets are 10 MHz [16], 190 MHz [11] and 1.37 GHz [10] for the aQ(8,7), sR(5,0) and aR(6,0) lines respectively. The significance of this choice of pump offset values and its effect on the laser gain will be fully developed in section II.7.

Fig. 3

Relevant energy levels of NH_3 for different pumping wavelengths. The solid arrowed lines indicate the absorbing transitions. The dashed arrowed lines show the expected lasing transitions.

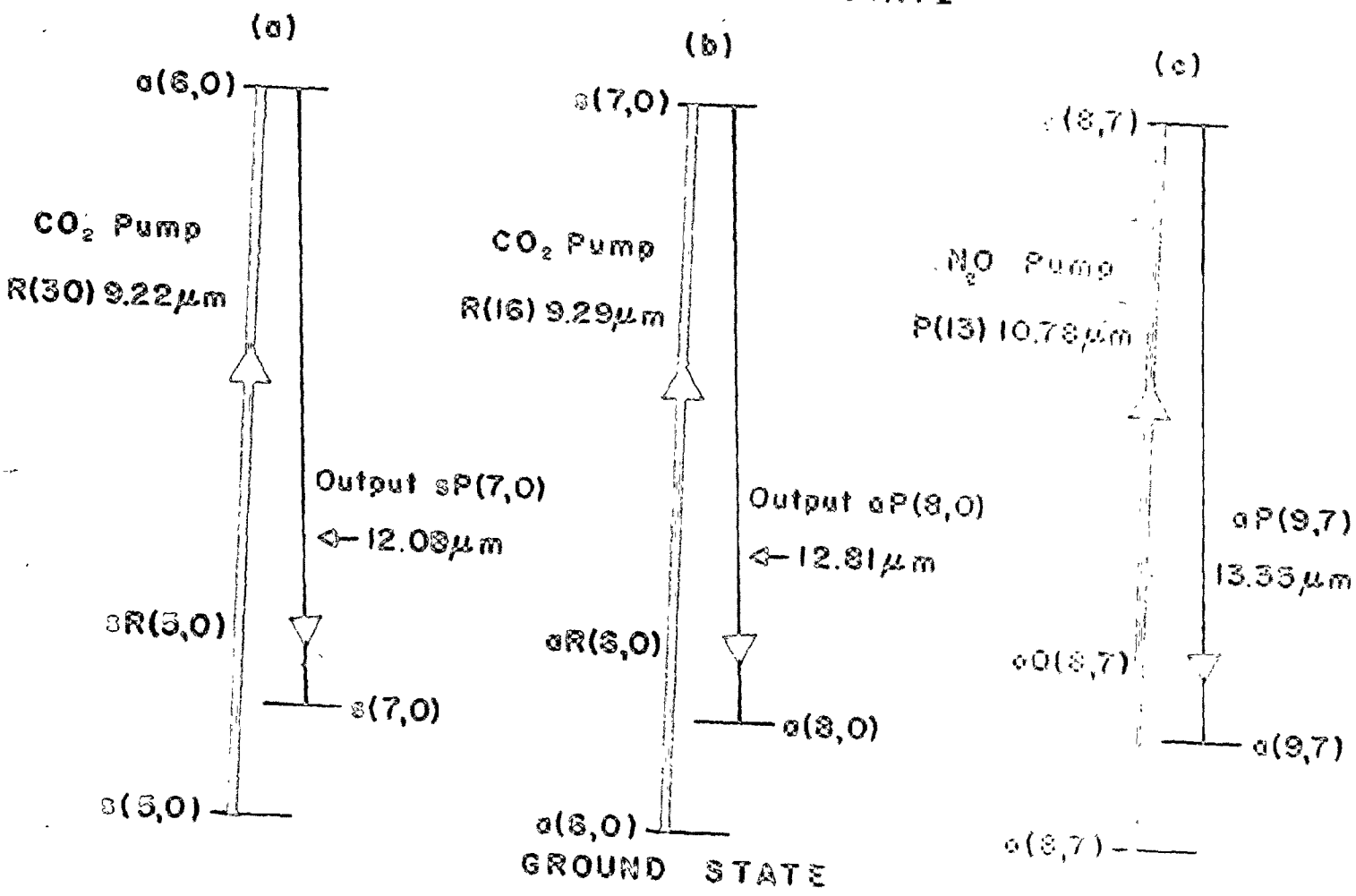
ν_2 VIBRATIONAL STATE
(a)
a(6,0)
CO_2 Pump
R(30) 9.22μm
Output sP(7,0)
← 12.08μm
sR(5,0)
s(7,0)
s(5,0)
(b)
s(7,0)
CO_2 Pump
R(16) 9.29μm
Output aP(8,0)
← 12.81μm
aR(8,0)
a(8,0)
a(6,0)
GROUND STATE
(c)
a(8,7)
N_2O Pump
P(13) 10.78μm
aP(9,7)
13.33μm
aQ(8,7)
a(9,7)
a(8,7)

II.5 The density matrix formalism

II.5.1 Introduction

Many models [17-21] have been proposed for the description of optically pumped IR (FIR and MIR)† lasers. Most analyses were carried out by means of rate equations [17,18, 21]. In such a model, the molecule is first excited under the influence of a resonant field and then contributes to the stimulated emission provided that a population inversion is achieved between the excited level and some lower state. Thus, in the rate equation model, we are dealing with two uncorrelated single photon transitions. However, this approach neglects contributions to the MIR gain due to multiphoton processes such as stimulated Raman emission. In the latter, a photon is simultaneously absorbed from the pump field and emitted into the MIR field. In many cases, the two photon process significantly alters the gain behavior. For example, for Doppler broadened transitions the Raman process gives rise to directional anisotropy in the MIR emission in the presence of strong coherent fields (pump and MIR) [22]. Other changes in the gain expression will be discussed later in this section. In contrast with the rate equation approach, a quantum mechanical treatment will simultaneously account for both the single photon process and the Raman-like process.

---

†The theory developed in this chapter is valid for both far infrared and mid-infrared lasers. For convenience, we will only refer to MIR lasers.

Such an approach is described below.

For our present purposes, an optically pumped MIR laser can be represented as a three level system, interacting resonantly with two coherent fields. Figure 4 gives the energy level scheme for such a system. A semiclassical treatment is used to describe the population dynamics of the three level system. From Maxwell's equations we obtain the classical electromagnetic field, while the time dependent Schrödinger equation is used in the density matrix formalism to describe the level populations.

II.5.2 A two field, three level system

The interaction of radiation with a molecule involves a Hamiltonian H where

$$H = H_o + V \quad . \tag{1}$$

H_o represents the unperturbed Hamiltonian of the molecule (no external field present) and V is the interaction energy. The perturbation considered here is the dipole interaction

$$V = - \vec{\mu} \cdot \vec{E}(\vec{r},t) \tag{2}$$

where $\vec{\mu}$ is the dipole moment matrix and $\vec{E}(\vec{r},t)$ the total electric field.

The time dependent behavior of the density matrix ρ is given by [20]

Fig. 4

Energy level scheme for an optically pumped MIR laser. Ω_{13} and Ω_{32} are the transition frequencies, ω_p and ω_f represent the field frequencies and ρ_{11}, ρ_{22} and ρ_{33} correspond to the population in levels 1, 2 and 3, respectively.

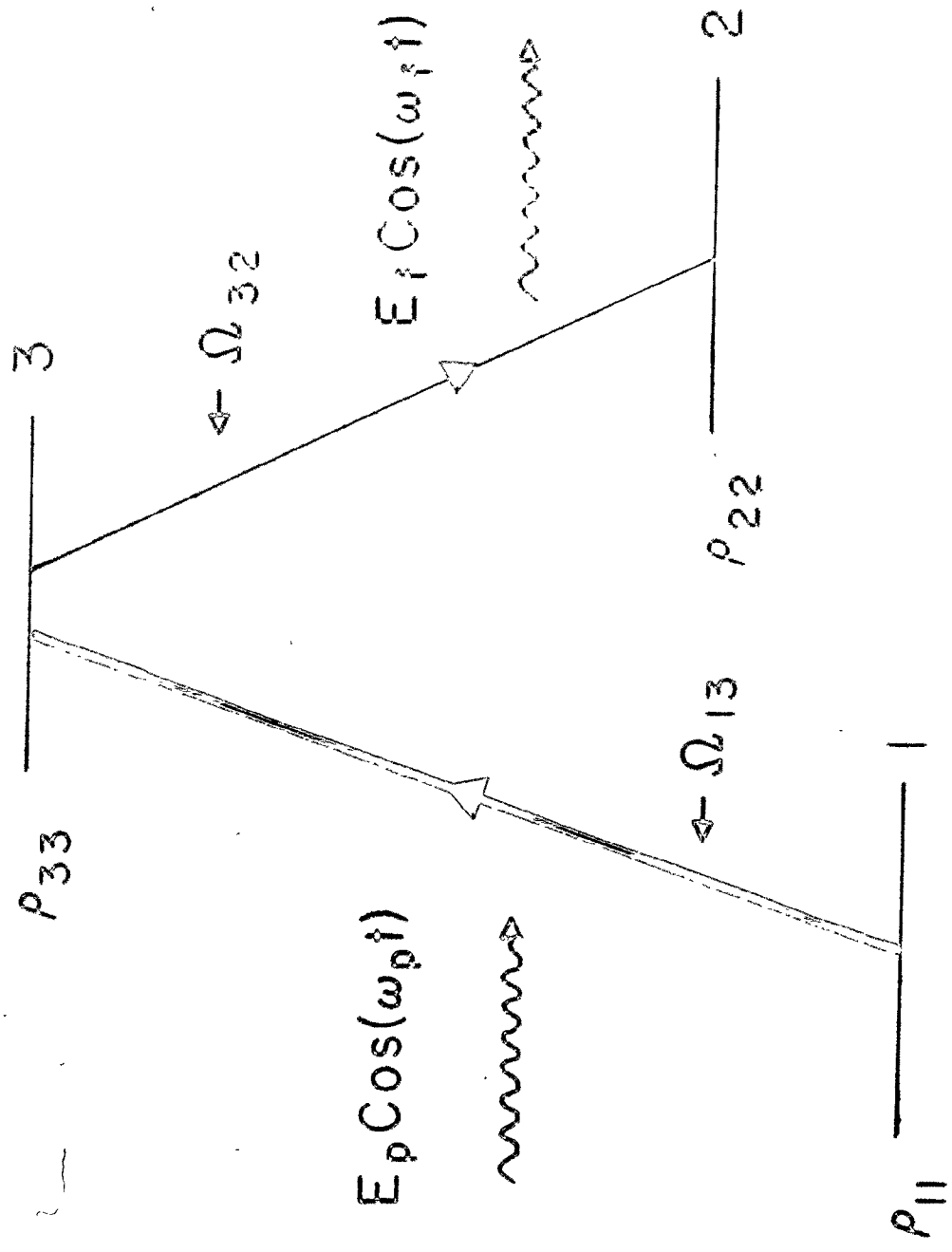
3
2
1
Ω_{32}
$E_r \cos(\omega_r t)$
Ω_{13}
$E_p \cos(\omega_p t)$
ρ_{33}
ρ_{22}
ρ_{11}

$$\dot{\rho}_{mm} = \tau_{mm}^{-1} (\rho_{mm} - \rho_{mm}^{o}) + \frac{1}{i\hbar} [\rho, H]_{mm} \quad (3)$$

$$\dot{\rho}_{mn} = \tau_{mn}^{-1} \rho_{mn} - \frac{i}{\hbar} [\rho, H]_{mn} \quad (4)$$

where m, n vary from 1 to 3. ρ_{mm} and ρ_{mm}^{o} give the probability for a molecule to be in the m state, in the presence and absence of an applied field respectively. The ρ_{mn}'s correspond to off-diagonal terms and are related to the radiation dipole. The decay constants τ_{mm}^{-1} and τ_{mn}^{-1} account for the molecular phase coherence times and are phenomenological terms. Only a full quantum mechanical treatment, where both the fields and the molecules are quantized, will introduce these decay times naturally. The τ_{mm}'s are called longitudinal relaxation times. They represent the time within which the population in the m'th level is restored to its thermal equilibrium value. The τ_{mn} parameters are the transverse relaxation times and characterise the loss of molecular coherence [24].

A general solution of equations (3) and (4), has not yet been obtained. However, these equations can be solved if certain approximations and assumptions pertinent to the specific MIR system under consideration are made. Recently, DeTemple [25] has solved the density matrix equations in the case of a three level system with homogeneously broadened transitions, interacting with two fields of arbitrary strengths.

Such an analysis is not directly applicable to a lower pressure gas where each molecule sees a Doppler shifted electric field. However, if the pump frequency is sufficiently far off resonance from the line center absorption such that homogeneous broadening dominates over Doppler broadening, we can treat the transition as homogeneously broadened [26]. Consequently, the DeTemple approach will generally be applicable to our work, even for low NH_3 pressure ($\sim$ 300 mTorr), provided the pump offset frequency exceeds several Doppler linewidths ($\gtrsim$ 90 MHz).

In order to understand the solution of equations (3) and (4), let us first examine the approximations and assumptions made by DeTemple [25].

(a) The DeTemple model assumes $\mu_{12} = 0$. This assumption is valid in our case as this dipole moment was effectively zero for all the transitions investigated [1].

(b) DeTemple assumes $\tau_{11} = \tau_{22} = \tau_{33} = T_1$ and that all τ_{mn} relaxation times can be represented by a single constant T_2. He further assumes $T_1 \sim T_2$. There is evidence that molecules in the $\nu_2 = 0$ and $\nu_2 = 1$, have somewhat different relaxation times and that $T_1 \neq T_2$ [27]. However, our present purpose is to extract the general behavior of the gain and we shall ignore these complications in our simple model.

(c) T_2 is typically $\sim$ 7 nsec Torr and the pumping time scale $\sim$ 300 nsec. At our working pressure (< 2 Torr),

we can apply a quasi-static solution i.e. to a first approximation, treat the pump intensity as being constant with time.

(d) The standard rotating wave approximation is used. Hence only the terms in which the molecular polarization and the electric field wave rotate together, are retained (i.e. terms containing $\omega_{ij} - \omega_{p(f)}$, see Fig 4). This is justified considering that we are working with optical frequencies.

(e) Finally, DeTemple uses the method of slowly varying amplitudes (SVEA) for ρ_{mn} i.e. assumes the amplitude of ρ_{mn} to vary little in an optical period ($T \sim 10^{-13}$ sec).

Under these conditions, the MIR gain coefficient is written as [25]

$$G_f = \sigma_{32}\{S_1(\rho_{33}-\rho_{11}) + S_2(\rho_{11}-\rho_{22})\} \qquad (5)$$

where σ_{32} is the homogeneously broadened cross section at line center for the 3 → 2 transition. S_1 and S_2, are related to lineshape functions and contain the resonance condition for maximum gain, power broadening effect and AC Stark shifts due to both the pump and the MIR radiation. The explicit expressions for S_1 and S_2 are given in Appendix A.

The significance of the two terms on the right hand side of equation (5) is crucial for the understanding of the laser dynamics. The first contribution is proportional to $(\rho_{33}-\rho_{22})$ and is called the inversion term. Most gain systems must produce a population inversion to obtain stimulated

emission (i.e. $\rho_{33} > \rho_{22}$). The first term of equation (5) fully describes the gain in inversion dominated lasers and can also be derived in a rate equation model. The second term deals with the two photon process i.e. the Raman contribution to the gain. This term allows gain to be created even in the absence of population inversion between levels 3 and 2.

The possibility of Raman-like laser transitions in off-resonant optically pumped MIR lasers was first discussed by T.Y. Chang *et al.*, in 1976 [7]. In many laser media both contributions can be present, although usually one term will dominate the other depending on the values of the various parameters (pump frequency offset, relaxation rates, pumping power, etc....). The fundamental differences between the Raman and inversion terms are discussed in detail in the next section which deals with the small signal gain.

II.6 Small signal gain

As stated in the previous section, the gain expression is valid for two fields of arbitrary strengths. The present work is concerned with the small signal gain which implies the absence of a saturating MIR field. In contrast to other researchers who employ high pumping intensities ($\geq$ 10 MW/cm^2), we have confined our work to relatively moderate pumping intensities of less than 100 kW/cm^2. Consequently, simplifications can be made to the algebraically complicated

expressions S_1 and S_2. This allows us to present a simple physical picture of the lasing processes. To this end, we now give several numerical values of the parameters used in S_1 and S_2, which are typical of the NH_3 transitions under consideration: $\mu_{13} \simeq \mu_{32} \simeq .12$ Debye, $T_2 \sim 8$ nsec at an operational pressure of one Torr and $0 \leq \frac{1}{2\pi} |\Omega_{31}-\omega_p| \leq 1.5$ GHz, where Ω_{31} and ω_p correspond to the line center transition and pump frequencies, respectively. These values combined with the weak field approximation permit us to simplify S_1 and S_2 (see Appendix A for further details). Hence, S_1 can be written as [25]

$$S_1 \simeq \frac{1}{T_2^2(\Omega_{32}-\omega_f)^2+1} \tag{6}$$

where Ω_{32} and ω_f are the line center transition $3 \rightarrow 2$ and the MIR frequencies, respectively. The inversion gain (proportional to S_1) exhibits a Lorentzian lineshape profile with a maximum value occuring at $\omega_f = \Omega_{32}$ i.e. at line center. S_2 is given by [21]

$$S_2 = \frac{\rho^2}{x^2} \frac{1}{T_2^2(\Omega_{21}-\omega_p+\omega_f)^2+1} \tag{7}$$

$$\left(\rho = \frac{\mu_{13} E_p T_2}{2\hbar} \quad \text{and} \quad x = T_2(\Omega_{31}-\omega_p)\right)$$

where E_p is the pump electric field.

The peak value of S_2 appears at $\omega_f = \omega_p - \Omega_{21}$ which corresponds to the Raman resonance condition. This constitutes a crucial difference between the two contributions: for the inversion term the MIR resonance frequency (ω_f) occurs at the line center of the lasing transition whereas in the Raman case the MIR resonance frequency is shifted from line center by an amount equal to the pump offset frequency.

If the pump intensity increases, we must take into account an additional effect, the AC Stark shift. This effect arises from the interaction of the pump electric field with the molecular dipole moment. In this model, it simply adds a factor $\frac{p^2}{x}$ to the Raman resonance condition. We will briefly discuss this small effect in Chapter V but presently we will concentrate our attention on the normal Raman case (i.e. $\omega_f = \omega_p - \Omega_{21}$).

We shall illustrate the expressions (6) and (7) by showing two extreme gain profiles. In the first, the inversion term dominates the Raman contribution and vice versa for the second profile. Figure 5 shows the graph of the normalized gain $\frac{G_f}{\sigma_{32}\rho_{11}^o}$ versus the MIR detuning frequency ($\Omega_{32}-\omega_f$) when a population inversion is assumed between levels 2 and 3. Our theoretical plot corresponds to the case of a small population inversion (i.e. $\frac{\rho_{33}-\rho_{22}}{\rho_{11}^o} \sim 4\%$) at a pumping intensity of 3 kW/cm^2. Much larger gains can be obtained if we saturate the pump transition (i.e. $\frac{\rho_{33}-\rho_{22}}{\rho_{11}^o} \sim 50\%$). The magnitude of the

Fig. 5

Gain profile for an inversion dominated laser. The normalized gain $\frac{G_f}{\Omega_{32}\rho_{11}^o}$ is plotted versus the FIR detuning $\Omega_{32}-\omega_f$. The values of the various parameters are: $\Omega_{31}-\omega_p = 600$ MHz (pump offset), $I_p = 3$ kW/cm^2 (pump intensity), $T_2 = 10$ nsec (relaxation time at a pressure of 1 Torr), $\frac{\rho_{33}-\rho_{22}}{\rho_{11}^o} = 4\%$ and $\frac{\rho_{11}-\rho_{22}}{\rho_{11}^o} = 18\%$. Note that the dominant gain occurs at line center and that a small Raman contribution is present at an offset of 600 MHz.

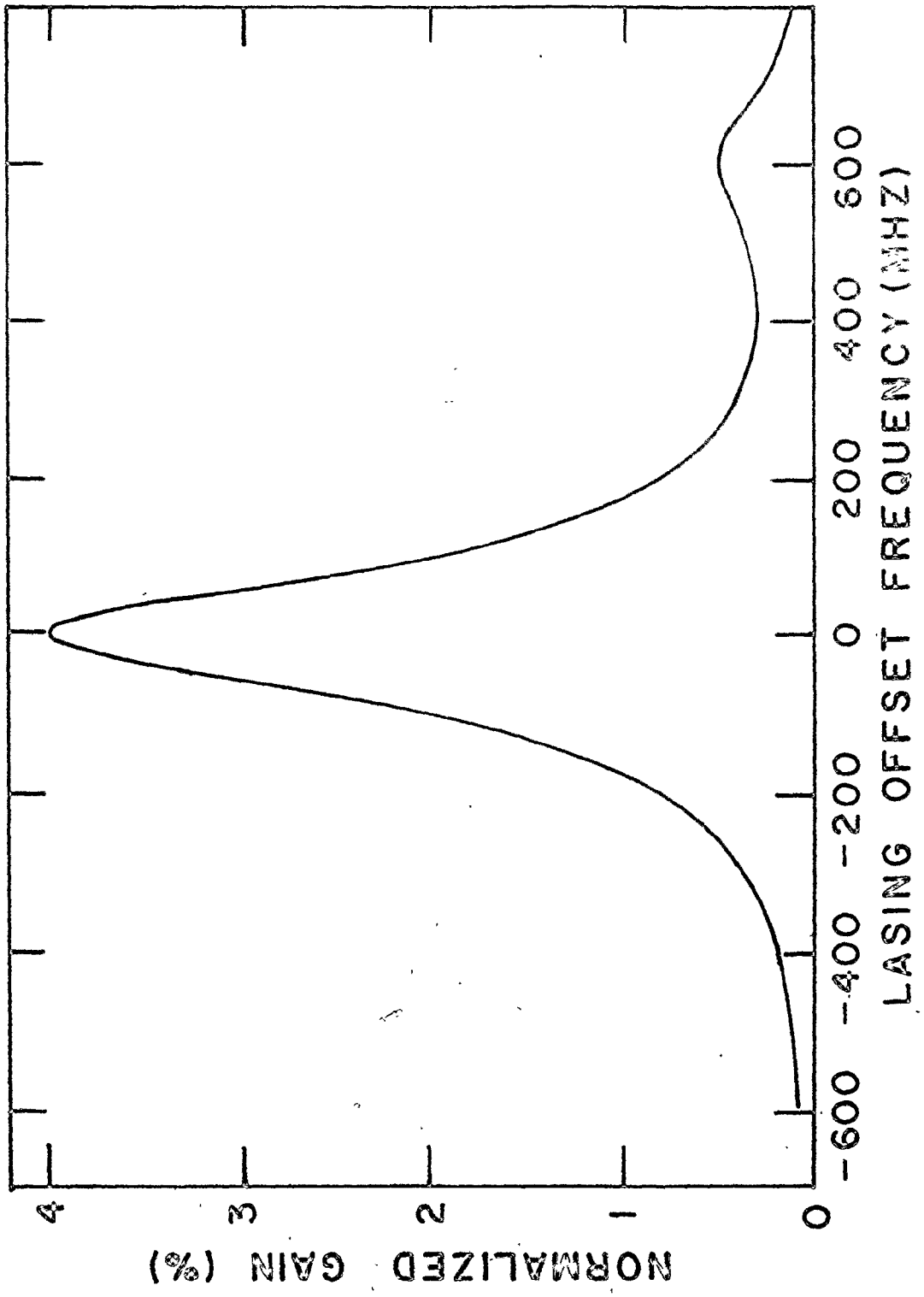
NORMALIZED GAIN (%)
0
1
2
3
4
-600
-400
-200
0
200
400
600
LASING OFFSET FREQUENCY (MHZ)

gain corresponding to these extreme population inversions, varies from 4%/cm to ∿ 30%/cm for typical NH_3 transitions. Another important feature to notice in Fig. 5 is the domination of the inversion gain over the Raman gain. The Raman gain occurs off resonance and its maximum value is only 1/8 of the peak inversion gain. Consequently, a laser with such a gain distribution would lase at line center, and large gain values would be observed. A quite different situation is depicted in Figure 6. Again the normalized gain $\frac{G_f}{\rho_{32}^{o} - \rho_{11}^{o}}$ is plotted as a function of the MIR detuning, but now we assume that no population inversion is produced between levels 3 and 2 (all the other parameters being kept constant). A considerable absorption now exists at line center which prohibits any lasing action at the transition frequency Ω_{32}. Gain is present at the Raman resonance frequency, with a peak value of ∿.6%/cm. Hence, at low pumping powers, this relatively small value of the Raman gain constitutes another major difference between the Raman and the inversion processes. Furthermore, equation (7) predicts a linear dependence of the Raman gain with the pump intensity. In contrast, for the inversion case, a very abrupt threshold exists as the pump intensity is increased. A small increment in the pump power can transform a strong absorbing medium into a system with large gain values ($\gtrsim$ 4%/cm).

Although the curves plotted in Figs. 5 and 6 are not based on experiment, but are simply calculated with our model,

Fig. 6

Gain profile for a Raman dominated laser. The normalized gain $\frac{G_f}{\sigma_{32}\rho_{11}^o}$ is plotted versus the MIR detuning $\Omega_{32}-\omega_f$. The parameter values used in the graph are identical to Fig. 5 except for the level populations: $\frac{\rho_{33}-\rho_{22}}{\rho_{11}^o} = -30\%$ and $\frac{\rho_{11}-\rho_{22}}{\rho_{11}^o} = 70\%$. Note the large absorption which now occurs at line centre and the small values of gain in the Raman region.

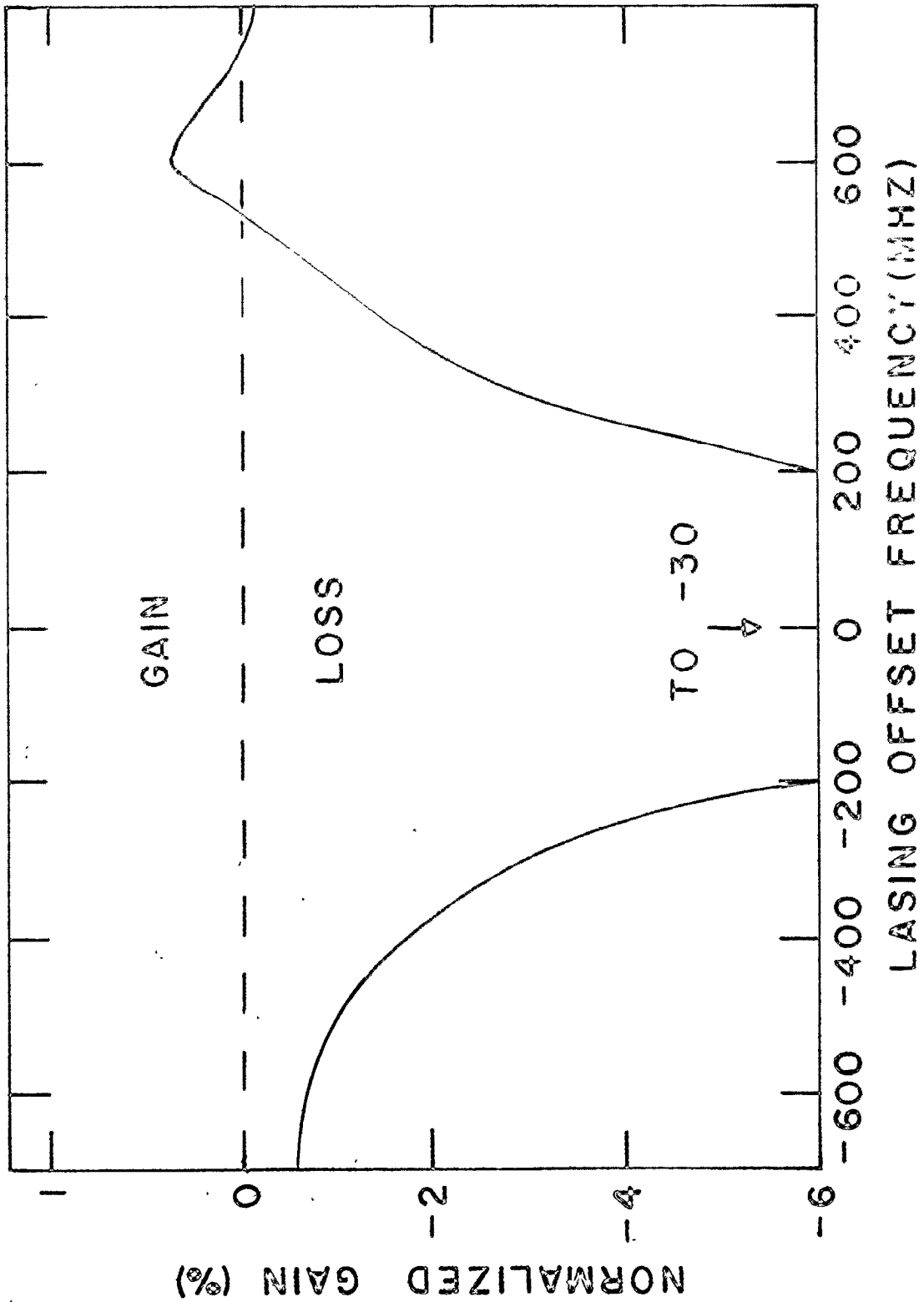
NORMALIZED GAIN (%)
1
0
-2
-4
-6
-600
-400
-200
0
200
400
600
LASING OFFSET FREQUENCY (MHZ)
GAIN
LOSS
TO -30

the figures display several dramatic differences between the Raman gain and the inversion gain. These basic distinctions will remain as long as we stay within the approximations of weak pump fields. In Chapter V, we exploit these differences to demonstrate conclusively that the NH_3 MIR lasers investigated in the present study are Raman lasers.

In summary, the chief differences between Raman and inversion gain are:

(i) In the Raman case, the lasing frequency is shifted off line center by an amount equal to the pump offset. Inversion lasing occurs at line center.

(ii) An inversion process will generally produce gain from 4%/cm to $\sim$ 30%/cm. Just above the threshold gain value (i.e. when gain initially exceeds cavity losses) any slight increase in pump power will give rise to a substantial increase of the gain.

(iii) In the absence of inversion gain, typical Raman gain will be relatively small ($\lesssim$ 2%/cm at low pumping powers). Moreover we expect the Raman gain to be linearly proportional to the pump intensity and thus no dramatic change with pumping power will occur.

CHAPTER III

EXPERIMENTAL APPARATUS

III.1 Introduction

In this chapter, a detailed description is given of the experimental apparatus. The pump laser, a helical pin-pin discharge system, is described. The merits of the TE laser as a tool for optically pumping a molecular gas are discussed. The important features of our MIR resonator are presented, and details are given of the optics and detectors. Finally, we give a general description of the MIR laser operation.

III.2 The helical TE laser

Our research utilizes a helical resistor pin-pin laser to optically pump the ammonia gas. The first TE (transversely excited) CO_2 laser was developed by Beaulieu [28], who employed a linear pin-pin discharge arrangement. Subsequently, different methods were developed to obtain a transverse excitation of high pressure gas mixtures (e.g. E-beam systems and double discharge preionization schemes). Although more powerful TE CO_2 lasers exist, the helical pin-pin laser was found to be well suited to the present investigation, for the reasons described below.

The helical array results in a gain distribution with cylindrical symmetry and thus produces laser output in the fundamental TEM_{oo} mode [29]. Such a Gaussian profile is required to mode match the pump laser radiation into the MIR resonator. Optimum mode matching will reduce the pump power needed to create MIR lasing. In order to produce a stable optically pumped laser, we must maintain a reasonably constant peak pump power. The helical TE laser pulse was reproducible on a pulse to pulse basis ($\sim \pm 10\%$). The pump power was readily controlled by varying the pressure inside the TE laser. Several hundred watts of peak output power were easily available for CO_2 gas mixtures below 100 Torr. Such powers were well in excess of the threshold pumping power required for typical NH_3 pressures used. A definite advantage of the helical TE laser over more powerful and consequently higher pressure TE lasers, is its narrower gain bandwidth. A narrow gain bandwidth gives a well defined laser output wavelength, and thus more stable pumping. For all these reasons, the helical laser was found to be well suited as an optical pumping source.

The TE pin-pin discharge system employed here is basically the same as that used by Reid [30]. The laser cavity is formed by a mirror and a grating, separated by 1.5 meters. At one end of the cavity, a partially transmitting mirror couples out the CO_2 radiation whereas at the opposite end of the resonator a copper replica grating (150 ℓ/mm) enables us

to select a single CO_2 laser line. The grating was mounted in a Littrow configuration. Fundamental mode operation was ensured by limiting the internal beam diameter to $\sim$ 8 mm. Figure 7 shows a typical CO_2 pulse, at a total gas pressure of 90 Torr. The CO_2 pulse was monitored with an Au-Ge detector, using the zeroth order reflection off the grating. This detector has a risetime of $\sim$ 2 nsec when operated into a 50 Ω load.

Variation of the total pressure of the gain medium alters the CO_2 pulse shape. For example, an increase of the gas pressure from 30 Torr to 90 Torr, decreases the full width at half maximum (FWHM) of the pulse from 500 nsec to 200 nsec. Furthermore, the length of the pulse tail (arbitrarily chosen to be when the pulse height falls off to $\sim$ 5% of its initial peak value) was reduced from 60 μsec to 8 μsec. Consequently, care was taken to keep the pressure of the TE laser constant for any given series of measurements, in order to produce identical pumping conditions.

III.3 Optically pumped MIR laser

Figure 8 is a schematic diagram of the experimental apparatus. The NH_3 cell is a short pyrex tube 27.5 cm long, in contrast with the typical $\sim$ 1 m tube length used in most optically pumped MIR and FIR lasers [31-34]. Such a short cell enables us to focus tightly the pump radiation into the MIR cavity, while maintaining a reasonably constant CO_2 beam diameter along the entire tube length. Two NaCl Brewster windows

Fig. 7

Typical CO_2 laser pulse at a total gas pressure of 90 Torr. (a) shows the entire pulse shape and (b) is an expanded view of the gain-switched spike.

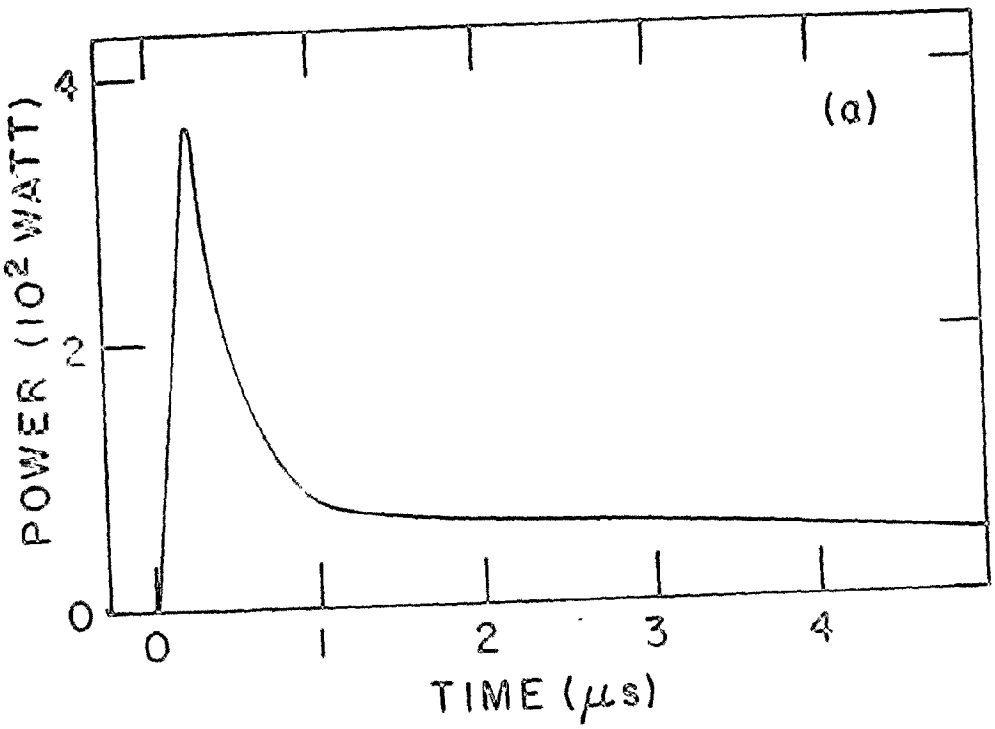
(a)
POWER (10^2 WATT)
0
2
4
0
1
2
3
4
TIME (μs)

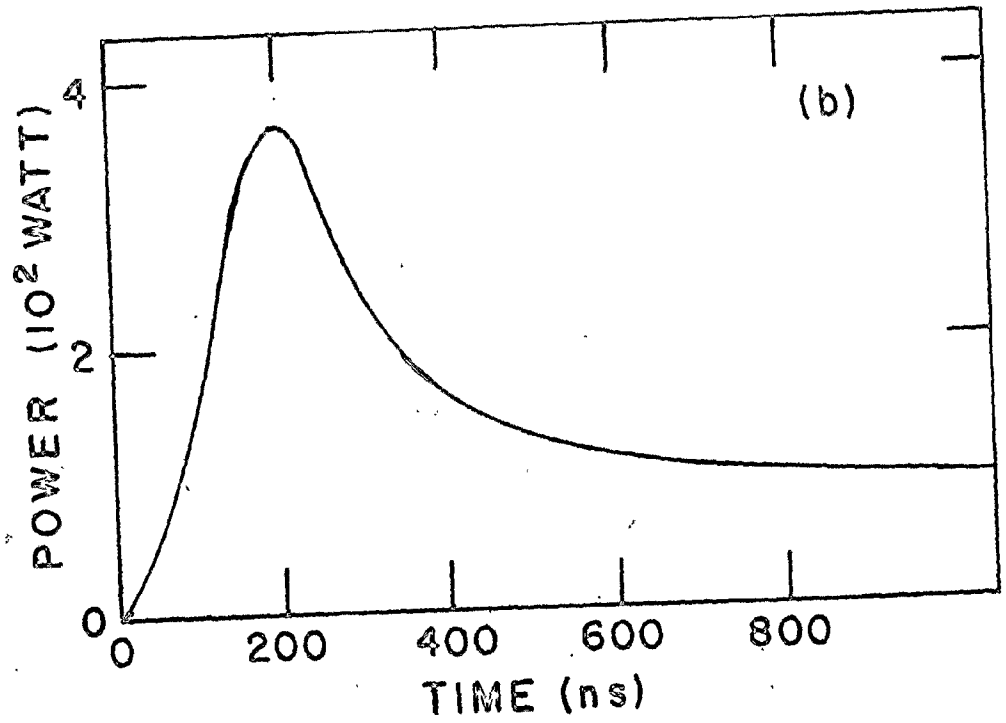
(b)
POWER (10^2 WATT)
0
2
4
0
200
400
600
800
TIME (ns)

Fig. 8

Schematic diagram of the experimental apparatus used for the optically pumped laser.

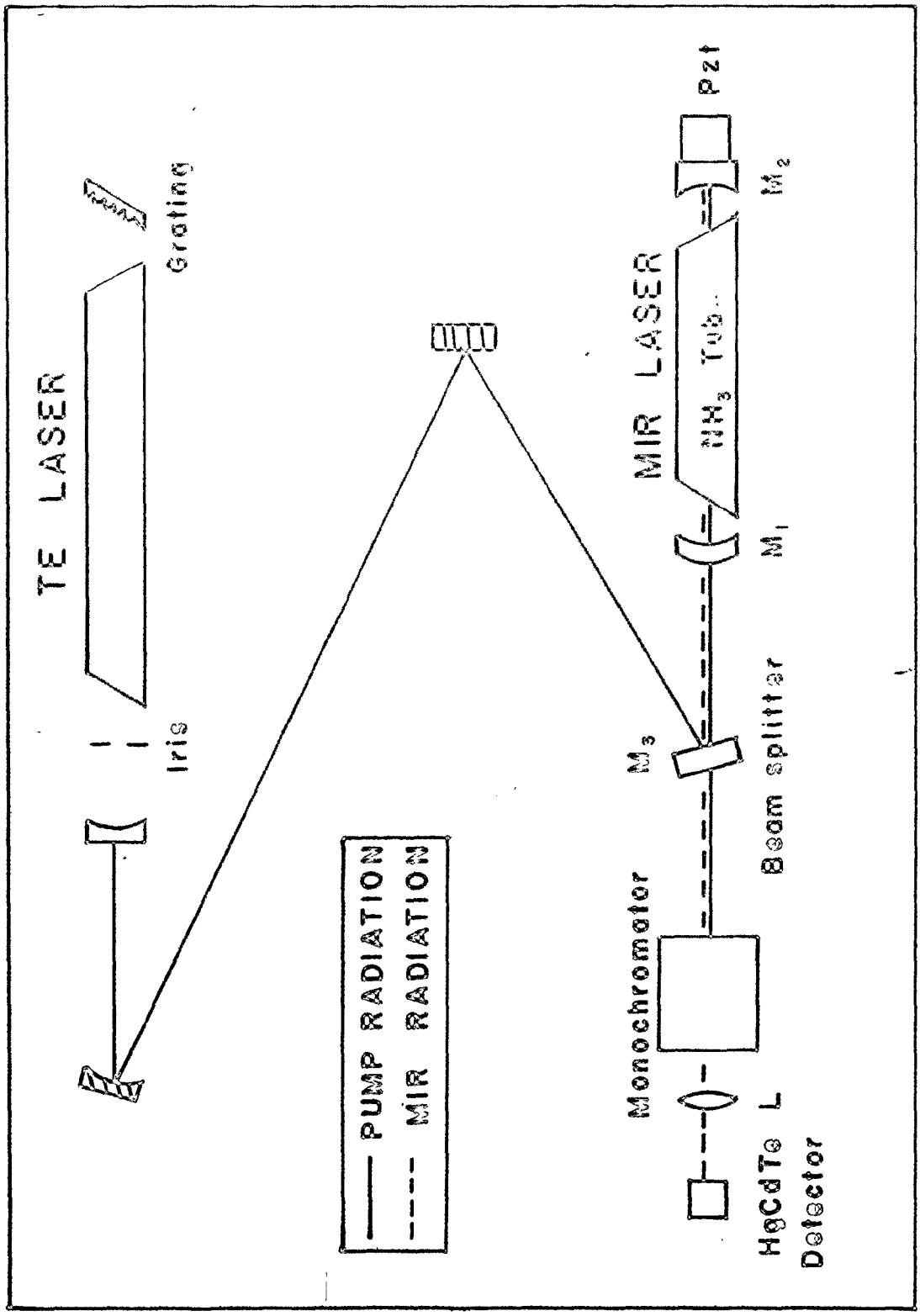
TE LASER
Grating
Iris
MIR LASER
NH_3 Tube
Pzt
M_2
M_1
M_3
Beam splitter
Monochromator
HgCdTe L
Detector
PUMP RADIATION
MIR RADIATION

sealed the ends of the 25 mm I.D. pyrex tube. Sodium chloride was employed because it transmits both the CO_2 and MIR wavelengths.

In the presence of water vapour, ammonia is known to attack copper, tin, zinc and their alloys. Stainless steel fittings and valves were therefore used throughout the gas-handling system. Care was taken to minimize leaks, and a liquid nitrogen cold trap prevented the NH_3 gas from entering the vacuum pump. The NH_3 pressure was monitored by two gauges. A barometrically compensated Edwards gauge (0-20 Torr) was situated at the inlet of the NH_3 cell. Low pressures were measured with an NRC 801 thermocouple gauge (0-1 Torr) located at the outlet of the pyrex tube. The latter gauge was calibrated for NH_3 against a capacitance manometer. High purity anhydrous ammonia was used (as supplied by Matheson) and the flow rate was controlled with a fine metering valve.

The output of the TE laser described in the previous section was focused by means of a concave (R = 1.4 m) gold coated mirror and coupled into the MIR resonator through a dichroic mirror (M_1) which transmits $\sim$ 50% of the incident pump power. M_1 is a wavefront corrected zinc selenide mirror (R = 1.6 m) whose high reflectivity, $\sim$ 94% at our MIR wavelengths ($\sim$ 12 μm), allows us to obtain a cavity with low losses (i.e. a high Q cavity). At the opposite end of the MIR resonator, a mirror M_2 is mounted on a piezoelectric translator to facilitate cavity length tuning. M_2 was varied

during the experiments, in order to study the relationship between the pump threshold power and the cavity losses (further details are given in Chapter V). To ensure maximum pumping efficiency, the CO_2 laser beam was closely matched to the TEM_{oo} mode of the MIR laser.

The MIR laser output was coupled from the resonator through M_1 which hence acts both as input and output mirror. The use of this configuration minimized the cavity losses by allowing a totally reflecting mirror to be placed at the other end of the cavity. The MIR output radiation was then directed through a beamsplitter (M_3, transmitting 15% at 12 μm) and was focused into a 1/4 m Jarrell-Ash monochromator using a .14 m radius gold coated mirror. The spectrometer was used to separate the MIR radiation from the CO_2 pump laser. At the exit slit, a 1" focal length Ge lens (L) focusses the MIR laser beam onto a HgCdTe detector, cooled with liquid nitrogen. This photoconductive device has a measured risetime of $\lesssim$ 50 nsec, taken directly at the output of the detector. The responsivity of the HgCdTe detector at 12 μm was estimated to be $\sim$ .2 V/W. This sensitivity could be increased by a factor 400 by employing an amplifier at the detector output. However, the risetime was then a factor of two slower. The amplifier was used only when high sensitivity was required. The signal was displayed on a Tektronix Type 545B oscilloscope with a 1A5 type plug-in unit ($\sim$ 8 nsec rise-

time). Hence, the risetime of the entire system was only limited by the detector ($\lesssim$ 50 nsec). Such a risetime was sufficient for all the required measurements.

Typical NH_3 laser pulses, obtained using the system previously described, are shown in Fig. 9. The upper trace (a) was taken near threshold operation i.e. using a minimum pumping power to produce a MIR pulse. Such pulses were obtained with pump peak powers as low as 20 Watts. The lower part of Fig. 9 (b) shows a MIR pulse when the pump power is well above threshold. In this case, the pulse lasted for $\sim$ 20 μsec. Even longer laser pulses were obtained ($\sim$ 500 μsec) by using a longitudinally pulsed CO_2 laser. Our observations indicate that the MIR pulse length is only limited by the pump pulse length. Such a result is obviously of crucial importance when considering the feasibility of an optically pumped cw laser and will be fully discussed in Chapter VI.

III.4 Summary

This chapter contains a detailed description of the experimental set up used throughout our work. As the pumping source, we use a TE laser. Typical MIR laser pulses, using our short resonator, were displayed and important features such as pump threshold power and pulse length were discussed.

The next two chapters are devoted to the discussion and resolution of the main issue of this thesis i.e. to find the actual mechanism responsible for the MIR gain.

Fig. 9

Time variation of two experimental MIR laser pulses. (a) represents a pulse near threshold operation whereas (b) corresponds to a laser pulse obtained with pumping powers well in excess of the threshold regime. Note the increase of the pulse length as the pumping power is increased.

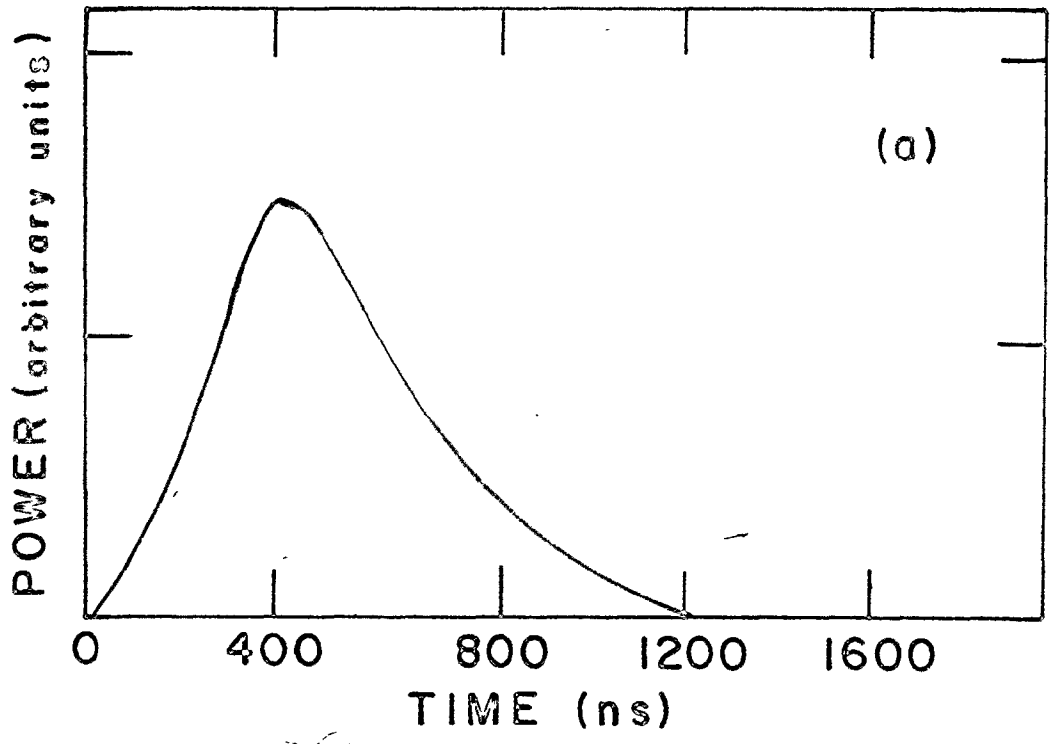
POWER (arbitrary units)
(a)
0
400
800
1200
1600
TIME (ns)

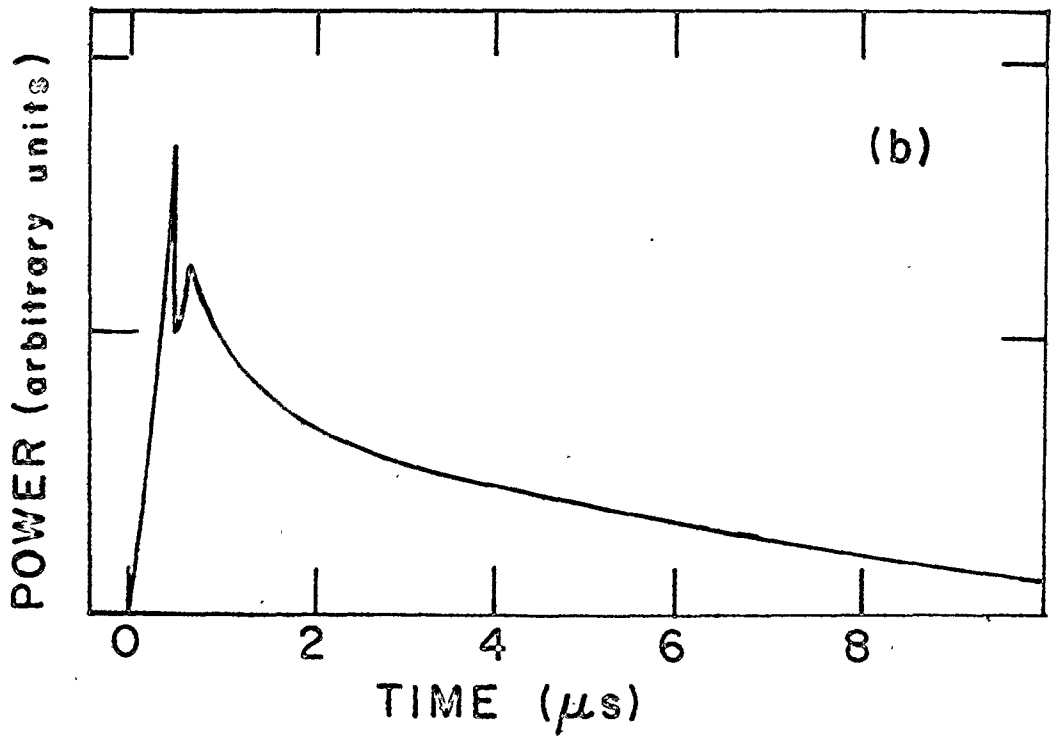
POWER (arbitrary units)
(b)
0
2
4
6
8
TIME (μs)

CHAPTER IV

SMALL SIGNAL ABSORPTION MEASUREMENTS

IV.1 Introduction

The work described in this chapter is aimed at characterizing the various parameters (pump frequency offsets, linestrengths and linewidths) of the CO_2 and N_2O pumped ammonia transitions introduced in Chapter II (see Fig. 3). In 1973, F. W. Taylor published calculated values of linestrength and pressure broadening parameters for the spectral lines in the ν_2 band of ammonia [9]. These calculated values are presently the best available. One objective of this chapter is to verify experimentally the accuracy of these calculations. Such information will then be used in the next chapter where linestrengths and linewidths for other NH_3 transitions are required. Furthermore, absorption measurements should confirm the observed pump offset frequencies [10,11]. As explained in Chapter II, an accurate knowledge of these offsets is important in a Raman laser. Finally, small signal measurements are necessary if we wish to determine the occurence of saturation in the pump absorption. Saturation measurements will be given in the next chapter. We are presently concerned exclusively with small signal absorption (i.e. absorptions measured at very low powers such that they are independent of the incident intensity).

The next section describes the technique employed to measure the absorption. Section IV,3 details the measurements of the absorption coefficient as a function of pressure. A comparison between the experimental results and the theoretical predictions is given in the final section.

IV.2 Experimental technique

A straightforward approach is used in this work to determine the pump absorption in NH_3. Figure 10 shows a schematic diagram of the apparatus. The CO_2 pump radiation is directed into a NH_3 cell and the transmitted intensity is monitored at the output of the cell, both with and without ammonia present. The absorption coefficient is then calculated from the Berr-Lambert law

$$\alpha = \frac{1}{L} \ln \left(\frac{I_o}{I_t}\right) \qquad (8)$$

where I_t and I_o are the transmitted and initial intensities respectively, and L corresponds to the absorbing length.

Accurate intensity measurements require a probe laser which is stable in both amplitude and frequency. The TE laser described in the previous chapter is not ideal for such measurements. The peak power varies by $\sim \pm 10\%$ on a pulse to pulse basis and there is a substantial frequency jitter due to the relatively high operating pressures ($\sim$ 80 Torr). These problems were overcome by replacing the TE laser by a cw CO_2

Fig. 10

Schematic diagram of the apparatus used for the small signal absorption measurements.

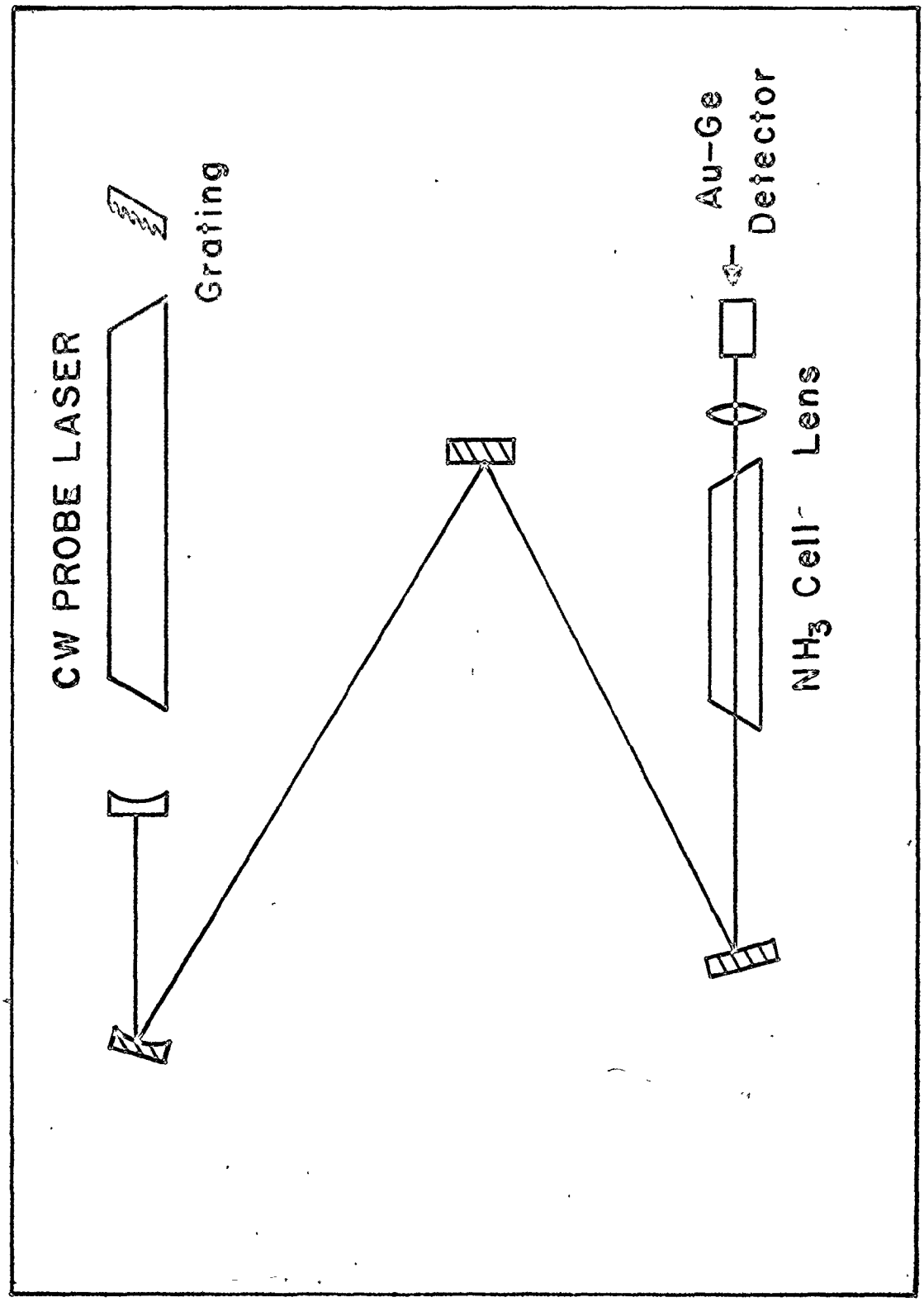
CW PROBE LASER
Grating
Au-Ge
Detector
Lens
NH_3 Cell

laser. At one end of the cw resonator a piezoelectric translator was used to control the cavity length. By optimizing the length to achieve maximum output power, we were able to obtain lasing at the CO_2 line center transition. Care was taken to minimize vibrations and thermal drifts. Consequently the laser power could be stabilized to better than ±5%, with negligible frequency jitter.

It was convenient to use a chopped rather than a continuous probe beam for the absorption measurements. This enables ac detection methods to be employed. Furthermore, chopping at a low duty cycle had two additional advantages. Firstly, the detector is protected from overheating and secondly, inaccuracies in the measured absorption caused by an increase of the gas temperature are eliminated. The intensity of the probe radiation was maintained at a sufficiently low level to avoid any intensity saturation in the absorption. This was verified by decreasing a given incident pump intensity by a factor $\sim$ 10 while the NH_3 pressure was kept constant. In each case, we measured an equal value of the pump absorption, confirming the absence of intensity saturation.

The signal transmitted through the NH_3 cell was focussed onto an Au-Ge detector. To increase the sensitivity of the detector (briefly described in Chapter III), a 10 kΩ termination was used. Due to the wide range of absorption coefficients measured, two different ammonia cell lengths were used,

a short cell of 2.4 cm and a larger one having a length of 27.5 cm.

IV.3 Absorption measurements

The various pump offset frequencies of our three NH_3 transitions imply different behavior of the pump absorption with the NH_3 pressure. We can divide the pressure range into three regions. At very low pressure ($\lesssim$ 8 Torr) the width of the transition is dominated by Doppler broadening. The lineshape function is then a Gaussian and the absorption coefficient is given by:

$$\alpha_D(\nu) = \alpha_D(\nu_o) e^{-[\ell n 2(\nu-\nu_o)^2/\Delta\nu_D^2]} \qquad (9)$$

where the Doppler broadened linewidth (HWHM) is

$$\Delta\nu_D = 3.58\times10^{-7}\ \nu_o\ \left(\frac{T}{17}\right)^{\frac{1}{2}}$$

for the ammonia at a temperature T(°K) and $\nu-\nu_o$ represents the offset frequency. The absorption coefficient at line center can be calculated from the known transition strength S (in $cm^{-2}atm^{-1}$) [35]

$$\alpha_D(\nu_o) = \frac{S\ A\ p}{\pi\Delta\nu_D} \qquad (10)$$

where p is the pressure (in atm) and A equals 1.48 for Doppler

broadened transitions. S and $\Delta\nu_D$ are taken at 300°K which corresponds to our experimental temperature.

When the pressure increases, molecular collisions make an increasing contribution to the transition broadening. At sufficiently high pressure (depending on the pressure broadening coefficient), the lineshape function is transformed into a Lorentzian profile

$$\alpha_L(\nu) = \alpha_L(\nu_o) \frac{\Delta\nu_L^2}{(\nu-\nu_o)^2+\Delta\nu_L^2} \tag{11}$$

where $\Delta\nu_L$ is the self broadening width (HWHM) and varies linearly with the pressure, $\Delta\nu_L = \beta p$. The absorption coefficient at line center is now given by [35]

$$\alpha_L(\nu_o) = \frac{S}{\pi\Delta\nu_L} \tag{12}$$

and is independent of the pressure because both S and $\Delta\nu_L$ are proportional to the pressure.

At intermediate pressure, the width of the transition is a combination of both effects (Doppler and pressure broadening). The lineshape is the convolution of a Gaussian profile with a Lorentzian function. The result is called a Voigt function [36]

$$\frac{\alpha_V(\nu)}{\alpha_L(\nu_o)} = a\pi^{\frac{1}{2}}V(x,a). \tag{12}$$

where $$a = \frac{\Delta\nu_L (\ell n 2)^{1/2}}{\Delta\nu_D} \quad , \quad x = \frac{(\nu-\nu_o)(\ell n 2)^{1/2}}{\Delta\nu_D}$$

and $$V(x,a) = \frac{1}{\pi} \int_{-\infty}^{\infty} \frac{a e^{-t^2} dt}{a^2+t^2} \quad .$$

Tabulated values of V(x,a) are available [37].

The total absorption of the probe beam is given by the sum of the contributions from all the NH_3 transitions. In practice, this sum is restricted to a few transitions near the probe frequency, all other contributions being negligible.

The aR(6,0) transition in the ν_2 band of NH_3 was the first transition studied (see Fig. 3). The R(16) line of the CO_2 9 μm band has an observed separation of 1.37±.15 GHz from the aR(6,0) line center. This offset is in good agreement with the value 1.23 GHz, calculated from the most recent molecular constants of NH_3 given by Shimoda *et al* [38]. This large offset (compared to a Doppler width of 48 MHz), ensures that at all pressures the measured pump absorption is dominated by Lorentzian broadening. We can therefore compare the theoretical Lorentzian expression (11) against our experimental measurements. A knowledge of three parameters is required: $(\nu-\nu_o)$, S and $\Delta\nu_L$. The linestrength and linewidth of aR(6,0) were taken from Taylor's calculated values [9]. Figure 11 shows the absorption coefficient α as a function of p^2. From equation (11), we would expect the absorption to vary as p^2 provided $(\nu-\nu_o)^2 >> (\beta p)^2$ which is a very good approximation in our

Fig. 11

Plot of the small signal absorption of the R(16) 9 μm band CO_2 laser line as a function of the square of the NH_3 pressure. Representative error bars are given for three points. The solid curve is a least mean square fit of the experimental points (o). The dashed line shows the theoretical absorption values calculated from Taylor's data [9].

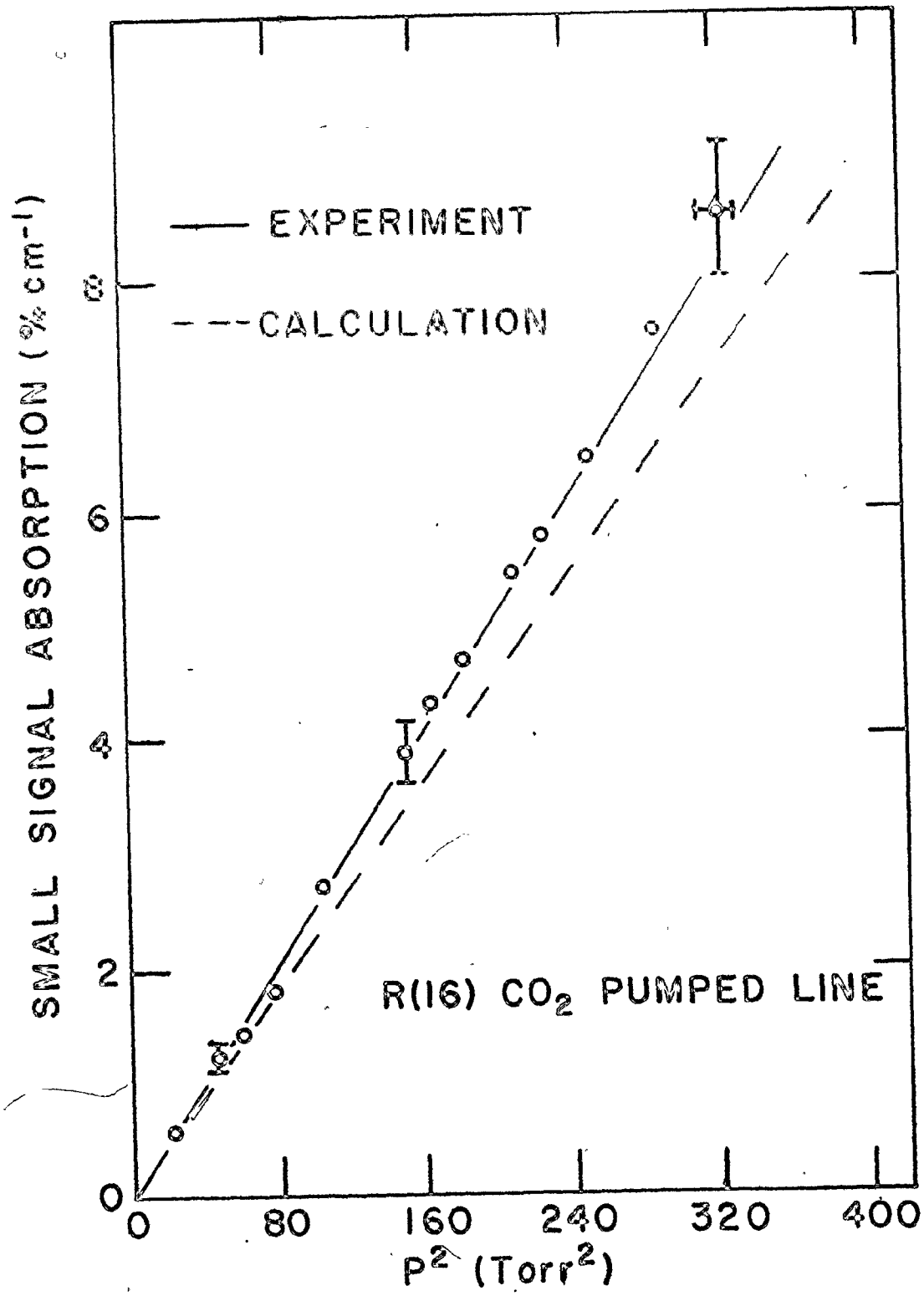
EXPERIMENT
CALCULATION
SMALL SIGNAL ABSORPTION (% cm⁻¹)
R(16) CO₂ PUMPED LINE
P² (Torr²)
0
2
4
6
8
0
80
160
240
320
400

pressure range. The solid curve of Figure 13 clearly shows a linear relationship between α and p^2, as predicted. This line was calculated using a least mean square fit to the experimental data. The result is:

$$\alpha = 2.65\times10^{-4}\ p^2 \quad (cm^{-1})$$

where p is in Torr. The dashed line represents the theoretical values of α calculated with Taylor's data ($S = 3.825\ cm^{-2}atm^{-1}$ and $\Delta\nu_L = .225\ cm^{-1}atm^{-1}$). Because the aR(6,0) line is an isolated absorption line, the contributions from all other lines were neglected. The resulting expression for the absorption coefficient is:

$$\alpha = 2.26\times10^{-4}\ p^2 \quad (cm^{-1}) \ .$$

By comparing the two slopes, we see that our experimental data are within 17% of Taylor's values. Furthermore, we have evaluated the product $S\Delta\nu_L$ from our experimental fit, taking the pump offset equal to 1.37 GHz. We obtained:

$$S\Delta\nu_L = 1.01\pm.07\ cm^{-3}\ atm^{-2} \quad \text{(experiment)}$$

whereas Taylor gives:

$$S\Delta\nu_L = .86\ cm^{-3}atm^{-2} \quad \text{(Taylor)} \ .$$

Thus, our experiment is reasonably close to the calculated values of Taylor (other researchers have observed even larger discrepancies with Taylor's predictions [39]).

A better agreement between our experimental results and Taylor's values is found for the R(30) pumped transition. The R(30) CO_2 laser line lies 190±5 MHz from sR(5,0) (the absorbing NH_3 transition of interest). Here, several adjacent lines in the sR(5,K) manifold must also be included in the theoretical absorption because of their proximity to the R(30) line, as shown in Fig. 12. This figure is a high resolution NH_3 absorption spectra, taken with a tunable diode laser. The trace shows the different sR(5,K) lines and their respective offset from the R(30) line [11]. A calibration of the frequency versus the laser diode current was achieved with the use of a Fabry-Perot etalon, allowing very accurate measurements of the pump offset frequencies (±5 MHz).

Once again, our objective is to compare the theoretical absorption (calculated with Taylor's data) with our experiment. The solid curve of Fig. 13 was obtained by a least mean square fit to the experimental data. The fit gives:

$$\alpha = 2.54\pm.18\times10^{-3}\ p^2\ (cm^{-1})\ .$$

The dashed line corresponds to the following equation, calculated from Taylor's data:

$$\alpha = \sum_{i=1}^{5} [sR(5,i)] = 2.42\times10^{-3}\ p^2\ (cm^{-1})\ .$$

As shown in Figure 13, the agreement between these two curves is quite good. Here again, the pump absorption was

Fig. 12

High resolution NH_3/CO_2 absorption spectra taken with a tunable laser diode near 1084.6 cm^{-1} [11]. The CO_2 absorption line is indicated by the arrow. The other absorption peaks belong to the sR(5,K) manifold of NH_3. The R(30)-sR(5,0) separation is 190±5 MHz.

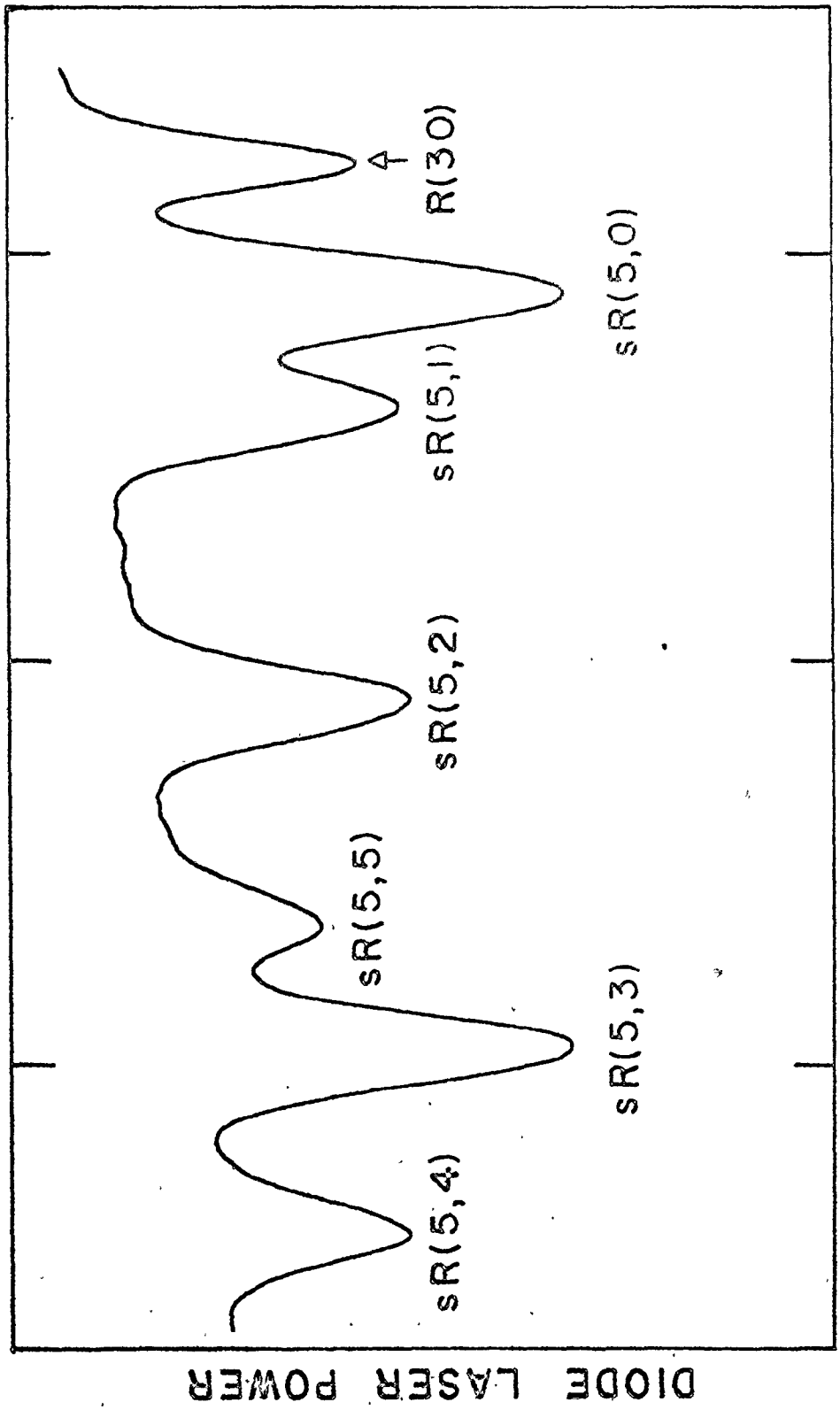
DIODE LASER POWER
sR(5,4)
sR(5,5)
sR(5,3)
sR(5,2)
sR(5,1)
sR(5,0)
R(30)
1084.68
1084.66
1084.64
WAVENUMBER (cm-1)

Fig. 13

Plot of the small signal absorption of the R(30) 9 μm band CO_2 laser line as a function of the square of the NH_3 pressure. The solid curve is a least mean square fit to the experimental values. Representative error bars are given for three points. The dashed line shows the theoretical values calculated from Taylor's data [9].

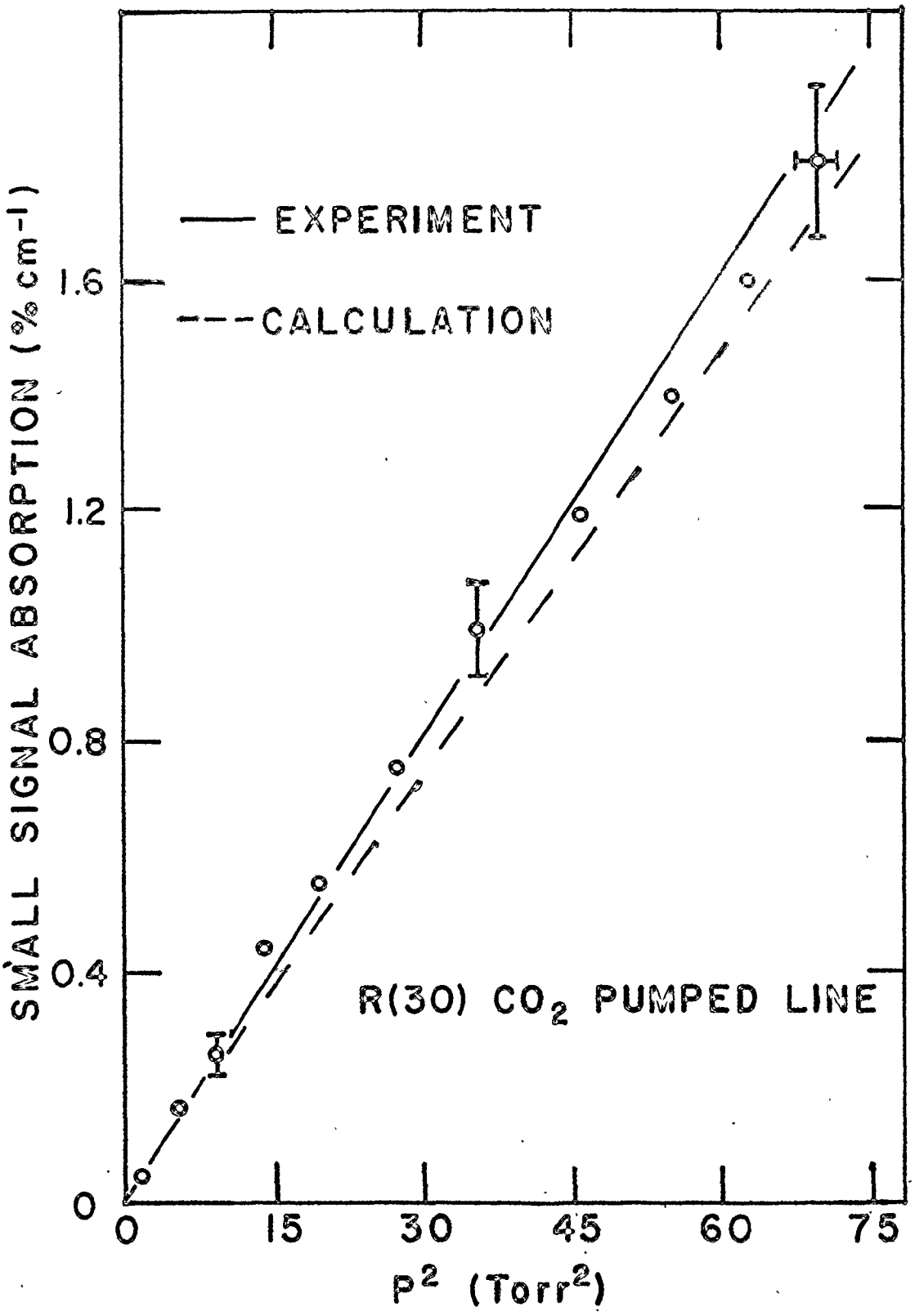
EXPERIMENT
---CALCULATION
R(30) CO_2 PUMPED LINE
SMALL SIGNAL ABSORPTION (% cm^{-1})
0
0.4
0.8
1.2
1.6
0
15
30
45
60
75
P^2 ($Torr^2$)

primarily due to Lorentzian broadening for our working pressure range (1 Torr $\leq$ p $\leq$ 9 Torr). This is clearly demonstrated by the linear dependence of α_{ℓ} as a function of p^2.

The third transition studied was the aQ(8,7) line. A close coincidence ($\sim$ 10 MHz) is known to exist between the aQ(8,7) transition and the P(13) laser line (10.78 μm) of the N_2O laser [16]. The conversion of the cw CO_2 laser into a N_2O laser was accomplished by simply replacing the CO_2 with N_2O in the gas mixture. The optics were unchanged, as the shift in wavelength (from 9.2 μm to 10.8 μm) only slightly affects the transmission of the mirrors.

Figure 14 shows the measured absorption as a function of the pressure. We can divide this graph into three regions. Below .75 Torr, the absorption coefficient is approximately proportional to p, which is characteristic of an inhomogeneously (Doppler), broadened transition. As the pressure increases, the pressure broadening parameter becomes comparable to the Doppler linewidth and mixed broadening occurs. The Voigt function (equation (12)) must then be used. At sufficiently high pressure ($(\beta p) >> \Delta\nu_D$), the absorption reaches a constant value $\alpha_L(\nu_o)$. The solid line of Fig. 14 represents our best fit, using a Voigt profile. The pressure dependence of the absorption coefficient is accurately described by the Voigt function. The following parameters were deduced from the fit: $a = .43$ p and $\alpha_L(\nu_o) = 1.16$ cm^{-1}. The calculated value of $\Delta\nu_D$ (41.8 MHz) combined with the above parameters,

Fig. 14

Measurements of small signal absorption of the P(13) N_2O laser line as a function of the NH_3 pressure. The solid curve represents the best fit of our experimental data (o) using a Voigt profile. Typical error bars are also shown. The dashed curve is the theoretical plot of the absorption using Taylor's calculated parameters. Experiment and theory have an identical pressure dependence and differ only by a scaling factor of 1.28.

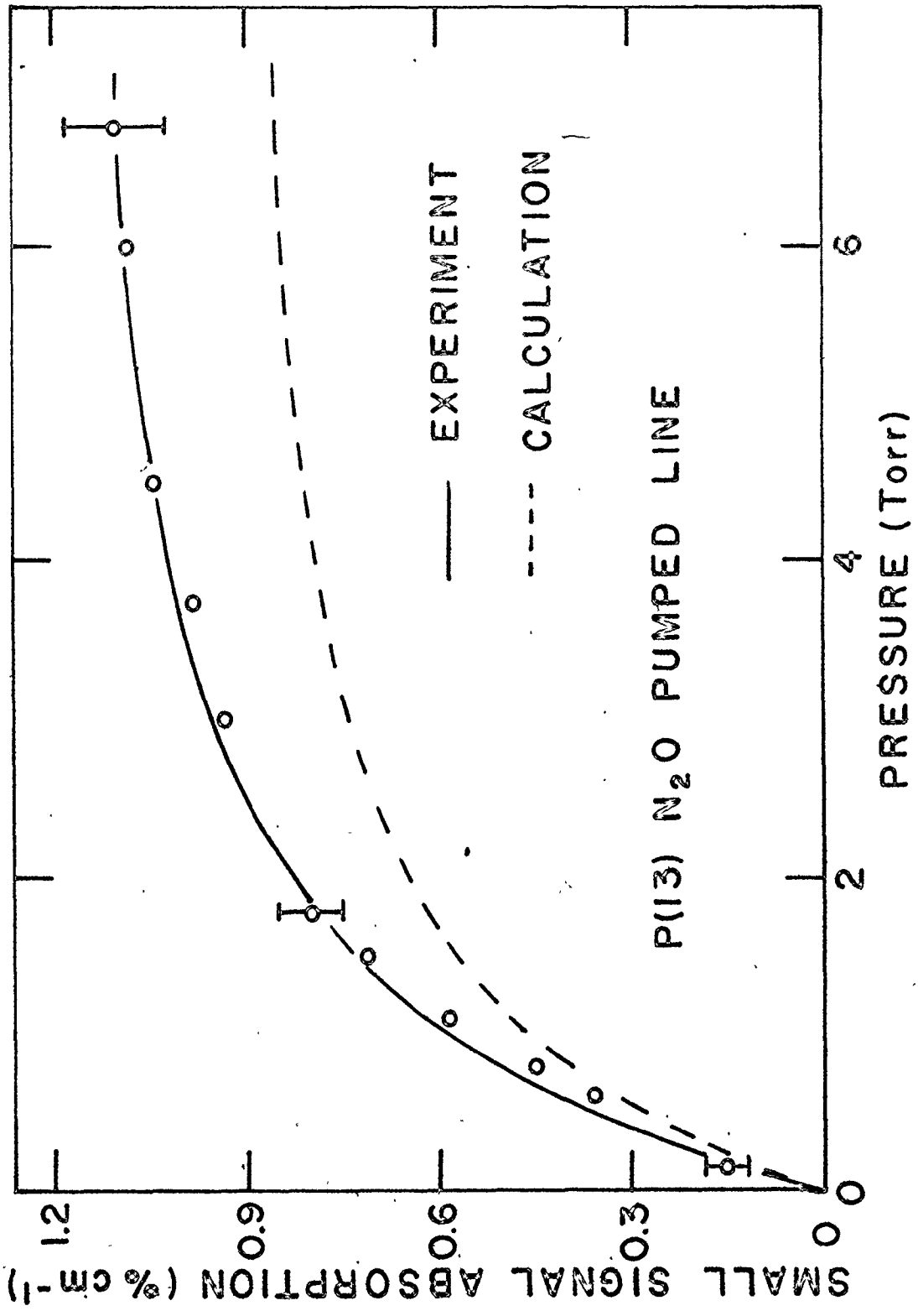
SMALL SIGNAL ABSORPTION (% cm⁻¹)
0
0.3
0.6
0.9
1.2
0
2
4
6
PRESSURE (Torr)
P(13) N2O PUMPED LINE
EXPERIMENT
CALCULATION

yield an homogeneous broadened linewidth equal to 21.6 MHz $Torr^{-1}$, and a linestrength of 1.99±.2 cm^{-2} atm^{-1}. The dasned curve of Figure 14 was calculated using $\Delta\nu_L$ = 21.6 MHz $Torr^{-1}$ and S = 1.55 $cm^{-2}atm^{-1}$ (from Taylor). The discrepancy between the two curves is only due to the difference in linestrength value. Once again, there is a reasonable agreement between our experiment and Taylor's calculated values.

IV.4 Summary

In this chapter, the small signal absorption of ammonia was investigated as a function of the pressure, using CO_2 and N_2O probe lasers. The theory described at the beginning of section IV.3 has accurately predicted the pressure dependence of the absorption coefficient for the various pump offset frequencies studied. Furthermore, theoretical predictions based on Taylor's calculated linestrengths and linewidths were generally in reasonable agreement with our experiment. The minor differences between our experimental results and Taylor's calculations are probably caused by uncertainties in the exact evaluation of linestrengths and linewidths employed by Taylor. These results are used in the next chapter where values of pump frequency offsets, linewidths and linestrengths are required. Also a knowledge of the small signal absorption coefficient is needed to determine the onset of pump saturation under MIR lasing conditions.

CHAPTER V

MEASUREMENTS OF MIR LASER CHARACTERISTICS

V.1 Introduction

In the previous chapter, we have discussed in detail two ammonia transitions pumped by a CO_2 laser (see Fig. 3 for the energy level diagram). Both transitions have led to lasing action in the 12 μm region. In 1976, T.Y. Chang and J.D. McGee reported a 12.81 μm optically pumped laser, using the R(16) line of the CO_2 laser (9.29 μm) [4]. In the same year, a 12.08 μm optically pumped laser using the R(30) line of the CO_2 laser (9.22 μm) was developed by Danielewicz *et al* [40]. Both groups employed high power CO_2 TE lasers (peak output powers of $\sim$ 1.5 MW) to pump these transitions. The principal aim of this chapter is to elucidate the basic process involved in these lasers.

Throughout the work described in this thesis, we have attempted to operate the 12 μm NH_3 lasers with minimum pumping powers. Two advantages clearly emerge from this. Firstly, our pulsed pump lasers will function at power levels similar to those commercially available in cw CO_2 lasers. Hence, we can use our results to examine the feasibility of an optically pumped cw MIR laser. Secondly, the use of low pumping powers in our NH_3 lasers will minimize coherent effects such

as AC Stark shifts and power broadening, permitting us to employ a relatively simple theory to predict the MIR gain. Consequently, our 12 μm cavity (see Chapter III) was designed for minimum losses and otpimum couplings. This approach has been successful, as can be seen by comparing our experimental pump threshold power (energy) with the minimum previously reported in the literature. For the R(16) pumped transition, we measured a threshold pump power of 600 Watts (160 μJ) in an optimised cavity. This threshold value is a factor of two lower than the lowest value found in the literature [41]. For the R(30) pumped transition, we achieved threshold pump energies as low as 6 μJ (20 Watts) compared to 700 μJ, the lowest value reported previously [41]. This threshold represents an improvement by a factor of more than 100.

The dramatic reduction in pump power needed to create gain as the offset changes from 1.4 GHz to 190 MHz led us to investigate a third possible NH_3 lasing transition, aP(9,7). The pumped transition is almost in exact coincidence (offset $\sim$ 10 MHz) with the P(13) line of the N_2O laser and it might be expected to give very low pumping thresholds. However, no lasing was observed even at peak powers as high as 700 Watts. Reasons for this behavior and its consequence will be fully discussed in section V.4.

In the previous chapter, we described small signal

absorption measurements. These results enable us to predict the percentage of pump power absorbed by the NH_3 gas under lasing conditions, provided no saturation takes place. An inversion laser would require the transfer of a large population from the pumped level to the upper laser state in order to overcome the high thermal population of our lower laser state (40% for the s(7,0) level and 28% for the a(8,0) level, relative to the pumped level). Such large population transfers would produce a concomitant reduction in the small signal pump absorption. The occurence of saturation in the pump absorption was investigated at NH_3 pressures and pump powers which were known to produce 12 μm lasing. Careful absorption measurements were taken at high powers and then compared with the small signal absorption values measured in Chapter IV. In all cases, the high and low power measurements were identical. The absence of pump saturation implies that no significant change takes place in the population levels, thus indicating the absence of population inversion. Such results strongly suggest Raman dominated MIR lasers, as opposed to inversion dominated lasers.

The rest of this chapter deals with experiments which confirm the Raman nature of the lasing process. In particular, we examine two further properties distinguishing a Raman laser from an inversion laser.

(i) In section V.2, careful measurements of the 12 μm lasing frequencies are made to determine if lasing occurs at line center (inversion case) or with a lasing offset frequency equal to the pump offset frequency (Raman case).

(ii) In section V.3, gain values are measured as a function of the pumping power. For a Raman laser we expect small gain values which increase approximately linearly with the pump intensity. In the inversion case, as a population inversion is approached, a small increase in the pump intensity will transform the system from large absorption to large gain values.

V.2 Lasing offset frequencies

Our objective is to determine the frequency offset between our 12 μm lasers and the corresponding line center of the 12 μm transitions. The method described in this section to measure the lasing offset frequencies is similar to the one employed in the previous chapter. Here, the 12 μm MIR output is used as the optical source and is directed into an NH_3 cell. The absorption of the 12 μm radiation is then measured as a function of the NH_3 pressure. The offset lasing frequency is calculated from our experimental absorption values, the theory presented in Chapter IV and Taylor's calculated parameters.

The measurement of absorption is a very efficient method of distinguishing between an inversion and Raman laser. In the first situation, a large absorption is expected because the lasing frequency coincides with the absorbing transition. However the absorption in the Raman case will be much smaller because of the lasing offset frequency (as long as $(\nu-\nu_o) \gtrsim \beta p$, see eq. 11).

The absorption of the 12.08 μm laser output in NH_3 was the first line to be studied. If the 12.08 μm radiation occurs off the line center of the sP(7,0) transition (see Fig. 3), we can predict the pressure dependence of the absorption coefficient by using the Lorentzian profile (eq. 11) and Taylor's calculated parameters for the sP(7,0) NH_3 transition. Taylor's data are known to describe with reasonable accuracy the 9 μm absorption. Consequently, his values for the 12 μm absorption will also be used because both the 9 μm and 12 μm regions are calculated by Taylor using the same band strength and self broadening cross section which imply a similar accuracy of the calculated parameters in the two regions. The predicted absorption coefficient is thus:

$$\alpha(\nu) = \frac{2.09\ (8.9p)^2}{(\nu-\nu_o)^2+(8.9p)^2} \quad (cm^{-1}) \qquad (13)$$

where $(\nu-\nu_o)$ represents the lasing offset frequency and p is the pressure in Torr. Figure 15 shows the experimental 12.08 μm absorption measurements as a function of p^2. As predicted

Fig. 15

Small signal absorption of the 12.08 μm MIR laser radiation as a function of the square of the NH_3 pressure. The solid curve is a best fit using a lasing frequency of 1.47 GHz and Taylor's data [9]. Typical error bars are shown. The dashed line indicates the large absorption which would be observed if the MIR laser was operating at line center.

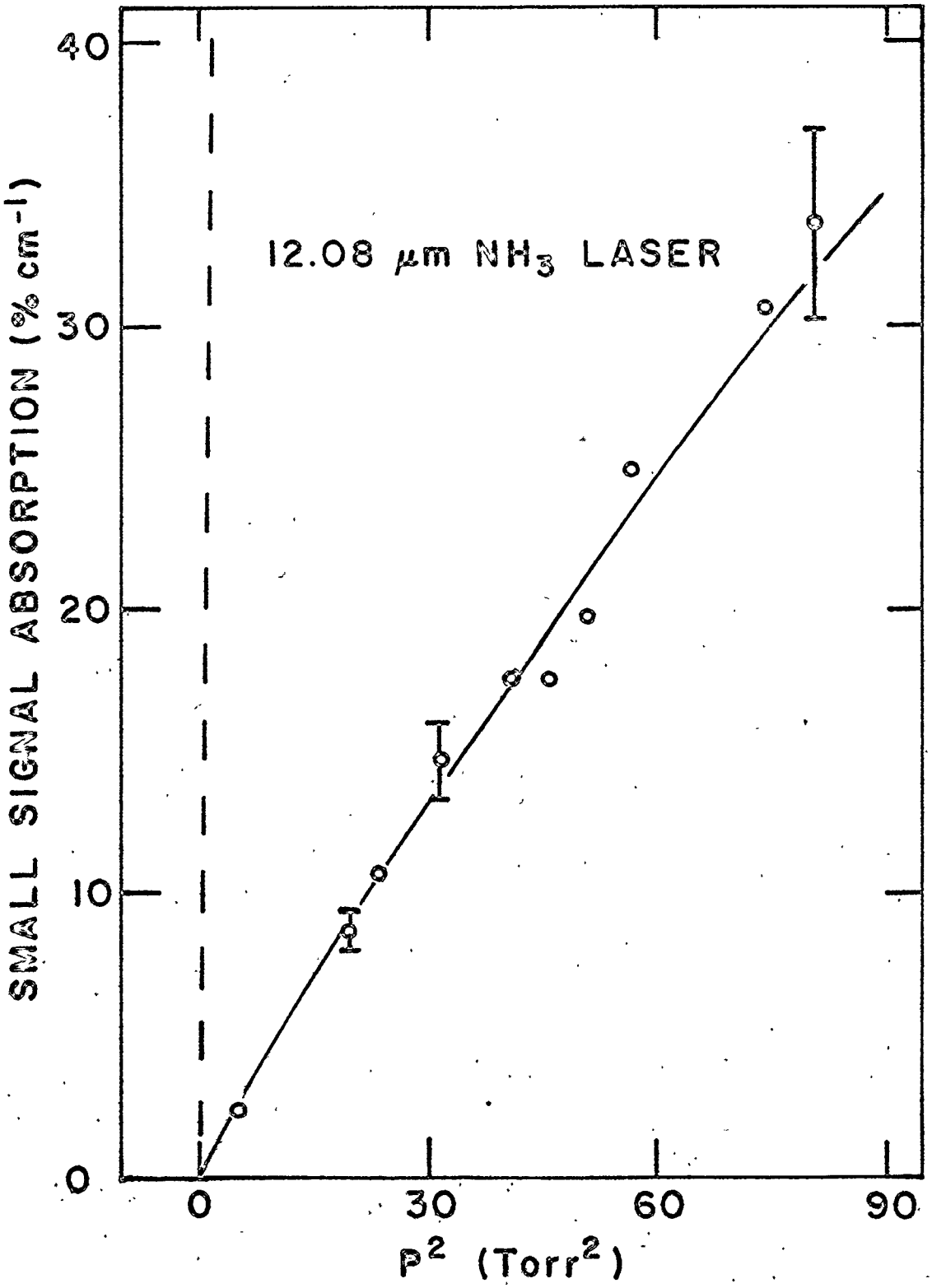
12.08 μm NH3 LASER
SMALL SIGNAL ABSORPTION (% cm-1)
P2 (Torr2)
0
10
20
30
40
0
30
60
90

by the Lorentzian profile (eq. (11), the absorption varies as p^2 at pressures below 7.5 Torr (i.e. when $(\nu-\nu_o) >> \beta p$). At higher pressures, the absorption deviates slightly from the p^2 dependence due to the pressure dependent term in the denominator of eq. (13). The dashed line corresponds to the calculated absorption assuming that the 12.08 μm lasing takes place at line center. Notice the striking difference between the dashed line and our experimental values. The solid curve of Fig. 15 is our best fit using eq. (13) and an offset frequency equal to 188 MHz. An error of ±15 MHz was evaluated for the lasing offset frequency. The experimental uncertainties in the absorption measurements were mainly caused by the shot to shot variation of the MIR laser. We were able to reduce the effect of such fluctuations by observing several pulses and systematically taking the ratio of the maximum absorbed MIR peak over the incident peak power. The 12.08 μm laser stability was good and resulted in an accuracy in the absorption measurements better than ±10%. An excellent agreement is found between the pump offset frequency, 190±5 MHz, and the lasing offset frequency, 188±15 MHz, deduced from our experimental data. The two values are nearly equal, hence confirming the Raman nature of the 12.08 μm MH_3 MIR laser.

Our next step was to measure the absorption of the 12.81 μm laser output in NH_3. For Raman lasing, the pressure dependence of the absorption coefficient is expected to

follow the expression below, obtained using Taylor's data for the aP(8,0) absorbing transition:

$$\alpha(\nu) = \frac{1.05\ (8.8p)^2}{(\nu-\nu_o)^2+(8.8p)^2}\ (cm^{-1})$$

where $(\nu-\nu_o)$ is the lasing offset frequency and p the pressure in Torr. The experimental absorption coefficients are plotted, versus p^2, in Fig. 16 for the 12.81 μm laser. Once again, we notice the same features discussed above for the 12.08 μm laser i.e. (i) a pressure dependence predicted by the Lorentzian profile (eq. 11) and (ii) a large difference between the dashed curve (calculated for line center absorption) and the experimental points. The solid line of Fig. 16 represents a best fit using equation (14) and taking the lasing offset frequency equal to 1.47 GHz. An accuracy of ±.21 GHz was estimated for this offset value. This larger relative error compared to the R(30) pumped laser is a result of the reduction in stability of the 12.81 μm laser. The higher pressure inside the CO_2 laser that was required to produce the needed pumping power increased the CO_2 pump frequency jitter. The increase jitter resulted in a more unstable 12.81 μm output. Consequently the accuracy of our absorption measurements was estimated to be ≈ 15%. Nevertheless, such an accuracy is more than sufficient for our present purposes. Indeed, our experimental lasing offset

Fig. 16

Small signal absorption of the 12.81 μm MIR laser radiation as a function of the square of the NH_3 pressure. The solid curve is a best fit using a lasing frequency offset of 188 MHz and Taylor's data [9]. Typical error bars are shown. The dashed curve indicates the large absorption which would be observed if the MIR laser was operating at line center.

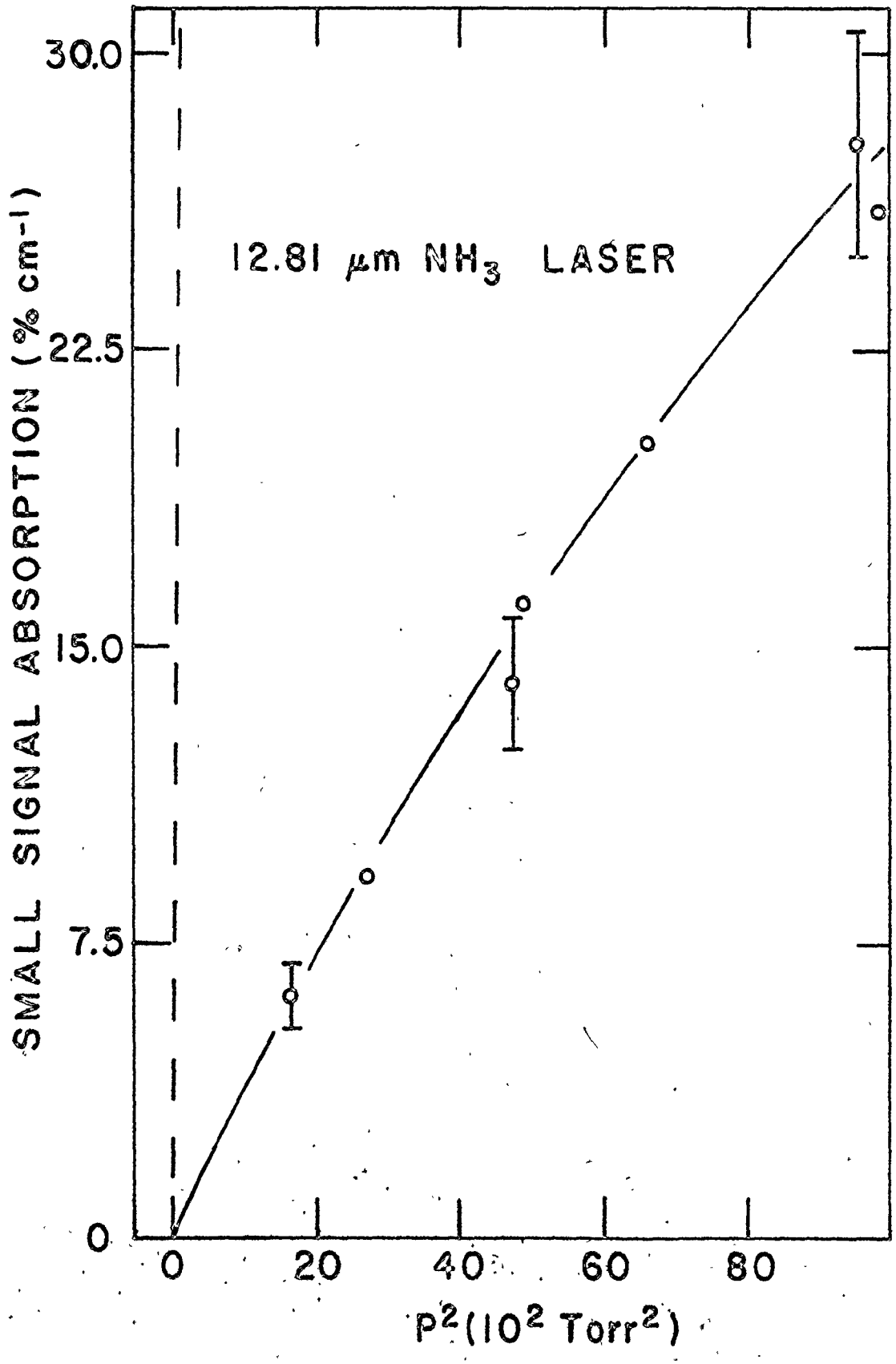
12.81 μm NH3 LASER
SMALL SIGNAL ABSORPTION (% cm-1)
30.0
22.5
15.0
7.5
0
0
20
40
60
80
P2(10² Torr²)

frequency of 1.47±.21 GHz agrees very well with the pump offset frequency 1.37±.15 GHz, thereby confirming the Raman nature of the 12.81 μm MIR laser.

In conclusion, the results described in this section provide the first direct experimental evidence of the Raman nature of the 12 μm lasers studied.

V.3 Small signal gain measurements

The measurement of small signal gain (S.S.G.) constitutes an independent approach to determine the process dominating the 12 μm MIR lasers. As stated in Chapter II, at low pumping powers, we expect relatively small Raman gain ($\lesssim$ 2%/cm), approximately proportional to the pump intensity whereas large gain values should be present in an inversion laser. Our aim is to measure the S.S.G. to determine which one of the two processes is relevant in our 12 μm lasers. Before giving the results obtained from this experiment, we will explain the method employed to evaluate the gain inside the MIR resonator.

The MIR small signal gain is defined as the gain in the absence of significant MIR field intensity. For a given cavity, the S.S.G. can be calculated from the threshold gain condition. This is the gain value at which a laser just starts to oscillate and thus, in effect, gives the S.S.G. In a simple steady state (cw) theory, the threshold gain condition

is given by [24]

$$e^{2\alpha_t \ell} R_1 R_2 L = 1 \qquad (15)$$

where $2\alpha_t \ell$ represents the round trip gain, R_1 and R_2 the reflectivities of the two laser mirrors and L includes other losses such as Brewster window losses and gas absorption per round trip. The exact amount of gain needed to offset these cavity losses is α_t.

For pulsed work, a correction must be made to take into account the excess gain (i.e. gain above the cavity losses) required to build up the MIR pulse from the spontaneous level to detectable levels. This excess gain is added to the threshold gain and the total value is the S.S.G.[†]. In many cases, the excess gain represents a large fraction (between 25% and 75%) of the total gain. An estimate of the errors this produces are given later in this section.

The evaluation of the cavity losses was straightforward. We can divide them into three groups: mirror transmissions, Brewster window losses and absorption of the MIR output by the NH_3 gas. The transmission of the different mirrors used in this experiment was determined with a Perkin Elmer spectrophometer (absolute error ±2%). Brewster window losses were estimated to be $\sim$ 1%/pass and the absorption

---

[†] Appendix B gives the details concerning the evaluation of the excess gain.

of the MIR radiation was calculated by extrapolating the absorption curves of the 12 μm lasers (taken in the previous section) at our working NH_3 pressures. An overall accuracy of ∿ ±3%/pass was estimated for the threshold gain values.

Gain measurements were first performed on the 12.08 μm laser. A steady flow (few cc/minute) of NH_3 at a pressure of ∿ 400 mTorr, was maintained throughout the gain measurements. The threshold gain was varied by decreasing the reflectivity (R) of the mirror M_2 situated at one end of the MIR resonator (see Fig. 8). To compensate for the higher cavity losses, the CO_2 pump threshold power was increased. This power corresponds to the minimum power needed to produce a MIR pulse and was measured with an accuracy of ±15%. The S.S.G. value was obtained by adding the threshold gain and the corresponding excess gain (accuracy of ±15%). Figure 17 shows the small signal gain of the 12.08 μm laser as a function of the CO_2 pump threshold power. The reflectivity of M_2 was varied from R = 98% to R = 65%. The gain approximately follows a linear relationship versus the pump power, as predicted by the theory of a Raman laser developed in Chapter II. Furthermore, notice the small absolute value of the gain, from .6 to 1.6%/cm, for the entire range of pump power (22 to 85 Watts). These two factors clearly show that the 12.08 μm laser is dominated by the Raman process.

Fig. 17

Small signal gain of the 12.08 μm laser versus the CO_2 pumping power. Also displayed are the experimental errors. Note the small values of the MIR gain and the linear dependence of the gain with the pump power.

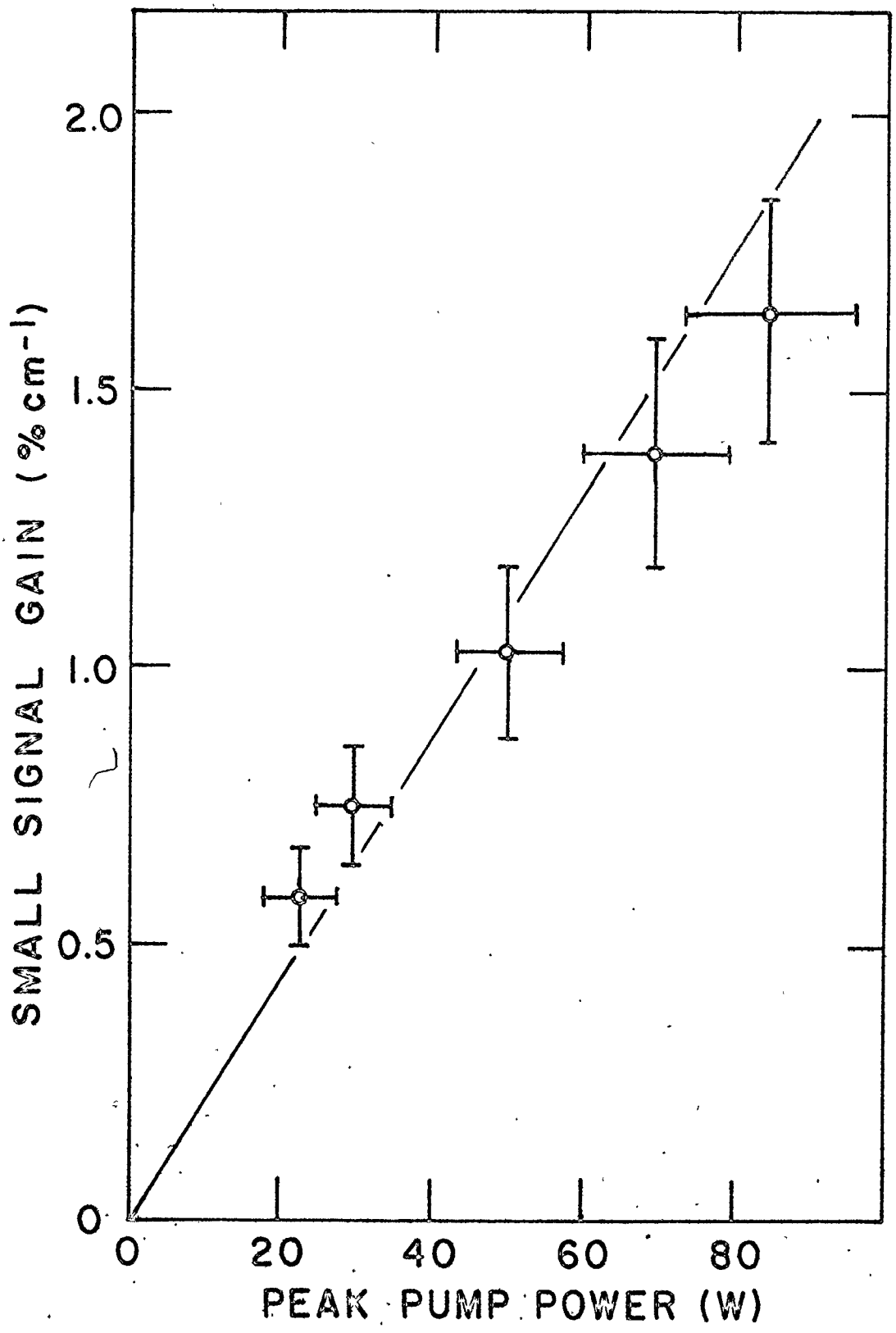
SMALL SIGNAL GAIN (% cm⁻¹)
2.0
1.5
1.0
0.5
0
0
20
40
60
80
PEAK PUMP POWER (W)

Gain measurements were next made on the 12.81 μm laser. Relatively short time delays were observed between the CO_2 pump pulse and the MIR pulse (between 500 nsec and 300 nsec). Large corrections in excess gain have resulted from these delays (see Appendix B). Typical cavity losses were 15%/pass while we have estimated excess gains a factor of three larger. Clearly, the accuracy of the small signal gain is limited by the accuracy of evaluating the excess gain. Estimates of excess gain are certainly much better than a factor of two, which is sufficient for our present purposes. We have determined a range of small signal gain values varying from $\sim$ 1.2%/cm to $\sim$ 2%/cm, while the pump threshold power was increased from 660 W to 6 kW. These results demonstrate two important points. Firstly, the gain values are relatively small and secondly, a ten fold increase in pumping power results in a gain increase by a factor of only 1.7. As discussed earlier, an identical pump power increase would lead to large gain if the inversion mechanism was responsible for 12.81 μm lasing. Hence, these facts confirm the Raman nature of the 12.81 μm gain.

The nonlinear relationship between the S.S.G. and the CO_2 power is to be expected as the pump power increases beyond several hundreds of Watts. In particular, our theoretical model treats each level as nondegenerate. This approximation is perfectly valid for degenerate levels as long as the

pumping intensity stays low ($\lesssim$ 30 kW/cm^2). At higher pumping levels, the M components of the angular momentum split and the gain is then distributed among the various M states hence, in effect, reducing the value of the peak gain. A more accurate description of the gain at moderate and high pumping power would clearly require a more complex model. However, a rough calculation indicates that the power level used for the R(16) pumped transition was sufficient to produce individual M Stark shifts up to 50 MHz from the Raman frequency. A consequence of such shifts is certainly a reduction of the peak gain value compared to the linear dependence predicted for nondegenerate levels, as the pump power increases.

V.4 The N_2O pumped transition

As discussed in the introduction the decrease of the pump threshold power as the pump offset diminishes led us to study the aQ(8,7) NH_3 transition. The P(13) N_2O laser line is almost an exact coincidence (pump offset $\sim$ 10 MHz) with the aQ(8,7) absorbing transition. In fact, this transition was the first optically pumped transition to generate FIR lasing in NH_3 (at 81 μm and 263 μm) [42]. Although another lasing transition is allowed, namely the aP(9,7) transition (see Fig. 18), laser action on this transition has never been reported in pure NH_3. Here, by pumping aQ(8,7), we have attempted to obtain lasing on the aP(9,7) line at 13.35 μm. We will first

discuss the particular aspects concerning the level diagram shown in Fig. 18 and next we will give the experimental results.

For the aP(9,7) transition a Raman laser would in effect lase at line center because of the negligible pump offset frequency. Consequently, in the absence of population inversion, the Raman process will not produce sufficient gain to overcome the large absorption (> 5%/cm) now present at the lasing frequency. The alternative is to create a population inversion. Because the lower 13.35 μm level in Fig. 18 possesses a large thermal population, we must strongly saturate the pump absorption to transfer a substantial population into the upper level s(8,7). Preliminary measurements have shown a strong saturation in the pump absorption for NH_3 pressure between 0 - 1 Torr and pump powers up to 500 Watts. We therefore searched for lasing at 13.35 μm using the laser cavity described in Chapter III. However, a hole coupling mirror was substituted for the dichroic mirror (M_1) due to a lack of suitable dielectric optics in the 13 μm region. The cavity was initially aligned and tested using the R(30) pumped transition and a CO_2 pump threshold of 200 W was obtained. We then switched to a N_2O pump laser and pumped NH_3 with powers up to 700 W. Lasing was not observed over a wide range of NH_3 pressures (30 mTorr - 2 Torr).

While the negative result was initially disappointing, it does illustrate a very important difference between the off-

Fig. 18

Energy level diagram relevant to the N_2O pumped transition. In addition to the FIR lasing transitions previously observed (81.5 μm and 263.3 μm), we show the expected MIR lasing transition (13.35 μm). The thermal level populations relative to a population of 100 in the pumped state (a(8,7)) are indicated beside each level.

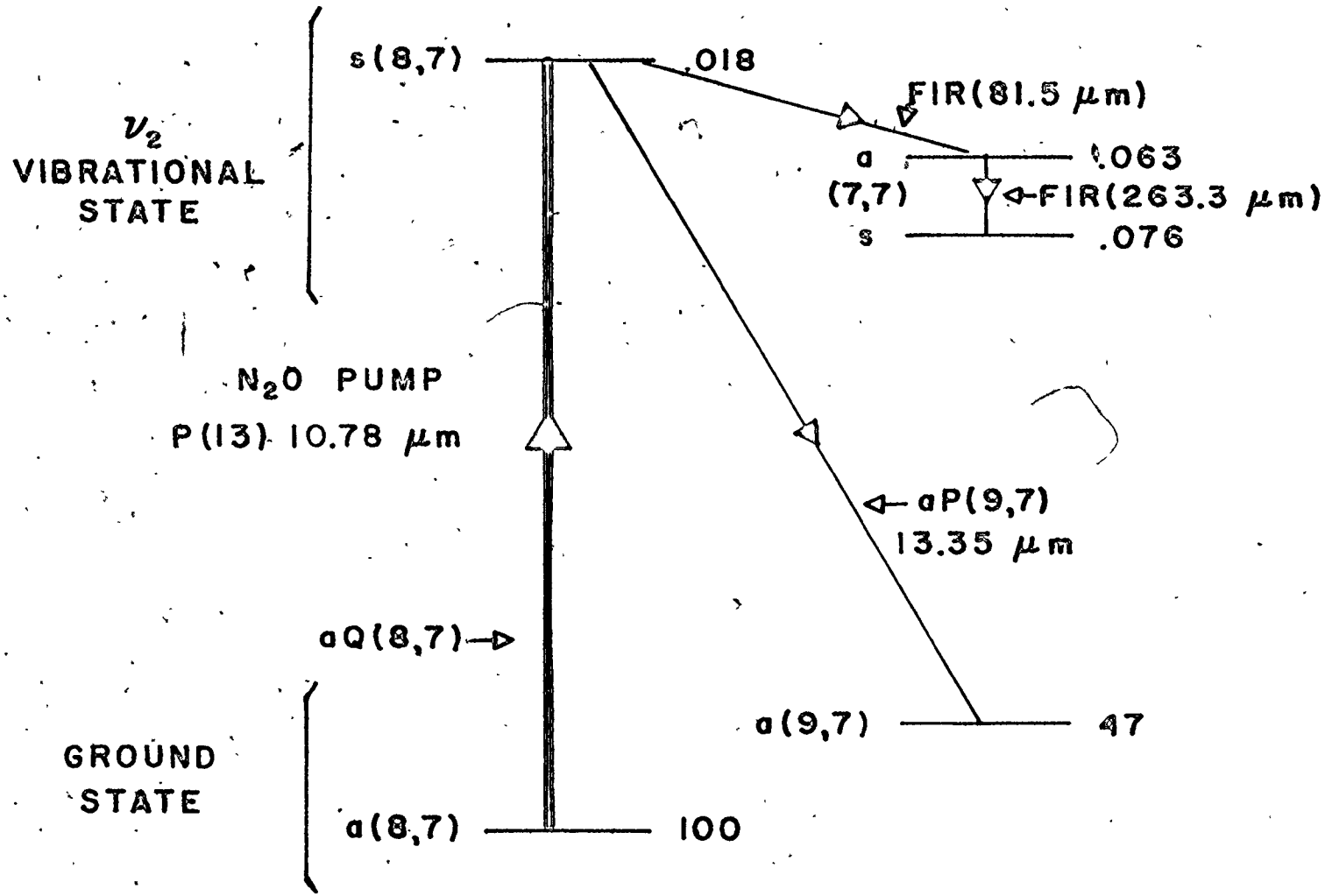
ν_2
VIBRATIONAL
STATE
s(8,7)
.018
FIR(81.5 μm)
a
(7,7)
s
.063
FIR(263.3 μm)
.076
N_2O PUMP
P(13) 10.78 μm
aP(9,7)
13.35 μm
aQ(8,7)
a(9,7)
47
GROUND
STATE
a(8,7)
100

resonant optically pumped MIR lasers and the more common FIR lasers. If we look at Fig. 18 for example, the 81 μm and 263 μm transitions have lower laser levels which are almost empty under thermal equilibrium. Consequently, a population inversion is very easy to produce. Optimum separation in a FIR laser requires then a very close coincidence between the pump frequency and the absorbing transition. In contrast, the large thermal population in the 13.35 μm lower level must be overcome by very high pump power if lasing is to take place at the line center. Thus, more efficient operation of the MIR laser can occur if the pump transition is offset from the lasing transition such that Raman lasing (without population inversion) is the dominant process. This simple picture was confirmed by our results on R(30) (threshold 200 W for a pump offset ∿ 190 MHz) and P(13) (threshold > 700 W for a pump offset ∿ 10 MHz). Although these results are not definitive they indicate the direction to follow for developing an optically pumped cw MIR laser, a point discussed in the next chapter.

V.5 Conclusions

In 1976, T.Y. Chang and J.D. McGee reported off-resonant infrared lasing without population inversion in NH_3. In the light of their results, they suggested that all previously reported off-resonant optically pumped MIR lasers (including the 12.08 μm and the 12.81 μm lasers) might be caused by a

Raman-type two quantum transition [7]. Since then, no experimental results were published to support their hypothesis. This thesis presents the first experimental evidence clearly demonstrating the Raman nature of the 12.08 and 12.81 μm MIR lasers, at relatively low pumping powers. This conclusion is based on three different experimental results: (i) the absence of saturation in the pump absorption, (ii) the lasing frequency offsets were accurately measured and are equal to the corresponding pump offset values and (iii) small gain values were measured and we observed the absence of a dramatic variation of the gain with the pump power.

This chapter has also shown the general behavior of the pump threshold with various pump offset values. By substantially decreasing the pump offset from 1.4 GHz to 190 MHz, we have reduced the CO_2 pump power threshold from 660 W to $\sim$ 20 W. On the other hand, a very close pump coincidence has indicated the need of higher pumping powers. These results are used in the next chapter to estimate an optimum pump offset which should provide minimum pump threshold power. Obviously, such an estimate is crucial to optimise the present system with a view to producing an optically pumped cw MIR laser.

CHAPTER VI

CONCLUSIONS

In this chapter, we outline the conclusions that can be drawn from the work reported in this thesis. This study has investigated off-resonant optically pumped NH_3 mid-infrared lasers at low pumping powers. Prior to this work, the fundamental mechanism governing such lasers was unclear. The main aim of this thesis was to demonstrate that the basic process responsible for lasing action is a Raman-type two quantum transition, as opposed to the more common single photon process.

In Chapter II, we identify the chief differences to be expected between a Raman and an inversion laser. We then compare the experimental behavior of the 12 μm lasers with calculations based on the theory of Chapter II and conclusively demonstrate the Raman nature of our MIR lasers.

This result is extremely important in the development of a good theoretical model for off-resonant low power pumped MIR lasers. The dominance of the Raman gain in these systems requires a model employing a quantum mechanical treatment which includes the multiphoton processes and coherent effects. A rate equation type model is totally inadequate because it considers only the single photon process. In Chapter II, we outline a simple density matrix model and find that

the mid-infrared gain expression can be divided into two contributions: the Raman and inversion terms. Such a model is well suited for most of our study but in Chapter V we detail some of the limitations which appear at high pumping intensity.

In addition to the above theoretical considerations, the Raman nature of the MIR gain has important practical consequences. If the frequency of the pumping laser is tuned then the MIR output will also tune because of the Raman process. Consequently, one can directly transfer the tunability of a 9 μm pump laser to the 12 μm region. This is a very practical consideration as tunable high pressure CO_2 lasers are now available. Another important aspect of the Raman process is the ability to create gain without population inversion. This enables us to obtain lasing at very low pumping powers. The observed threshold pump powers are now well within the range of conventional cw CO_2 lasers and pump power limitations should then not be an obstacle to the development of a cw 12 μm NH_3 laser. Such a laser would have a wide range of applications in spectroscopy, photochemistry or as a probe of 12 μm laser dynamics. We therefore have examined more closely the feasibility of cw operation by utilizing long pump pulses ($\sim$ 500 μsec) from a longitudinally excited CO_2 laser. Again, the results were encouraging and we observed MIR pulses of approximately the same length. This result confirms that the dynamics of the NH_3 system do not prohibit cw MIR lasing.

Before any serious attempt is made to obtain cw operation, the present system must be optimized. In particular, the NH_3 transition must be chosen so as to minimize the pump power requirements. The results presented in Chapter V emphasize the importance of the pump offset frequency on the pump power threshold. Decreasing the pump offset reduces the pump power threshold until the pump frequency gets close to the absorbing line center. Raman lasing is virtually impossible very near the line center due to the large absorption of the unpumped NH_3 gas and, unless the pump frequency is several Doppler linewidths offset from the line center, high pumping thresholds are required. Consequently, we estimate that the optimum pump offset lies in the range of 80 to 200 MHz. At room temperature, we predict an optimum pump offset of $\sim$ 100 MHz for NH_3, in the 12 μm region. Recently, T.A. Znotins *et al* [43] have produced efficient optically pumped NH_3 MIR lasers using low pumping powers, with pump offsets equal to 190 MHz, 140 MHz and 90 MHz. Their most efficient MIR laser was obtained by reducing the pump offset to 90 MHz. These results clearly support our predictions. Further investigations are needed and the NH_3 transitions used by T.A. Znotins *et al* [43] should be subjected to future studies. As a result of the work described in this thesis we are optimistic that a new cw laser can be developed.

In conclusion, this thesis has provided a better un-

derstanding of the laser dynamics involved in optically pumped MIR lasers. Our results are certainly not limited to the lasing transitions studied. Similar considerations will apply to other optically pumped molecules, lasing in the mid-infrared region. Consequently, it is hoped that this research will be of considerable value to the development of better optically pumped MIR lasers.

APPENDIX A

GAIN COEFFICIENTS

DeTemple has derived a gain expression in the case of a three level system interacting with two coherent fields of arbitrary intensities. This expression is given by [25]

$$G_f = \sigma_{32}\{S_1(\rho_{33}-\rho_{22})+S_2(\rho_{11}-\rho_{22})\}$$

where

$$\sigma_{32} = \frac{\omega_f(\vec{\mu}_{32}\cdot\hat{\varepsilon}_f)^2 T_2}{\hbar\varepsilon_o c}$$

is the homogeneous broadened line center cross section for the $3 \rightarrow 2$ transition. The other symbols are defined in Fig. 4 and Chapter II. The cross sections S_i are conveniently expressed with normalized variables defined to be [25]:

$$x = T_2(\Omega_{31}-\omega_p) \qquad y = T_2(\Omega_{32}-\omega_f) \quad \text{(detunings)}$$

$$P = \frac{\vec{\mu}_{13}\cdot\hat{\varepsilon}_p E_p T_2}{2\hbar} \qquad Q = \frac{\vec{\mu}_{23}\cdot\hat{\varepsilon}_f E_f T_2}{2\hbar} \quad \text{(fields)}$$

$$L(z) = z+i \quad \text{(lineshape)}$$

then

$$S_1 = \mathcal{J}_{ma}\left\{\left[1 + \frac{P^2-Q^2}{L(x-y)L^*(x)}\right]\frac{1}{L^*(y)\Delta}\right\}$$

$$S_2 = \mathcal{J}_{ma}\left\{\frac{-P^2}{L(x-y)L(x)L^*(t)\Delta}\right\}$$

where $$\Delta = 1 + \left[\frac{P^2}{L^*(y)} - \frac{Q^2}{L(x)}\right] \frac{1}{L(x-y)} .$$

These expressions are general and contain effects such as power broadening and AC Stark shifts due to both the pump and MIR fields. Simplifications to these complicated expressions can be made if we consider the typical experimental conditions used in this work. The numerical values given in Chapter II permit us to write $Q << 1$ and $\frac{P^2}{x^2} << 1$. Then $\Delta \simeq 1$ and

$$S_1 = \frac{1}{y^2+1} = \frac{1}{T_2^2(\Omega_{32}-\omega_f)^2+1}$$

$$S_2 \simeq \frac{1}{x^2(x-y)^2+1} = \frac{P^2}{x^2} \frac{1}{T_2^2(\Omega_{21}-\omega_p+\omega_f)^2+1} .$$

These expressions were plotted in Figs. 5 and 6, for certain population levels. If the pump intensity increases such that $\frac{P^2}{x}$ is not negligible compared to x, we have

$$S_3 \simeq \frac{1}{(y+\frac{P^2}{x})^2+1} \quad \text{and} \quad S_2 = \frac{P^2}{x^2} \frac{1}{(x-y+\frac{P^2}{x})^2+1} .$$

In this case, the inversion and Raman resonances have been AC stark shifted in opposite directions by an amount equal to $\frac{P^2}{x}$. Although, this term was negligible for most of the pump intensities used in our experiment, we have evaluated $\frac{P^2}{x}$

at the maximum power employed for the R(16) pumped transition. A maximum AC Stark shift of 50 MHz was calculated and the consequences of such a value are discussed in Chapter V.

APPENDIX B

DISCUSSION OF THE EXCESS GAIN USED IN CHAPTER V

In Chapter V, we have introduced a correction to the threshold gain caused by the use of pulsed pump lasers rather than continuous ones. This appendix discussed the evaluation of the excess gain required to produce a certain level of power inside the MIR resonator. We estimate than an in-cavity power of .1 W corresponds to the lower level at the beginning of our typical MIR pulse. If the MIR gain does not give rise to this minimum power no pulse will be detected. This power level is equivalent to 2×10^{10} MIR photons (ρ_f) in our cavity. A rough evaluation of the amplification factor needed to obtain 2×10^{10} photons from the spontaneous emission (ρ_i) gives $\frac{\rho_f}{\rho_i} \sim 4\times10^{8}$. For a time dependent gain, the ratio is also equal to:

$$\frac{\rho_f}{\rho_i} = \exp \int \alpha(t) \, \frac{L}{L'} \, c \, dt$$

$$\ell n\left(\frac{\rho_f}{\rho_i}\right) = \left(\frac{Lc}{L'}\right) \int \alpha(t) \, dt = \text{const. (gain}\times\text{time)}$$

Where L' and L are the resonator and active lengths respectively. Figure 19 shows the time dependent profile of the

Fig. 19

Time variation of the normalized 12.08 μm gain $\frac{G}{G_o}$. The cavity loss line corresponds to a MIR cavity with a mirror M_2 of reflectivity ∿ 98% (see Fig. 8). Excess gain, as defined in Chapter V, is indicated in the figure. The shaded area represents the (gain × time) product available for the amplification of the MIR pulse from spontaneous noise. At threshold, this full area is required to produce an observable MIR pulse which consequently appears at a delay time of 700 nsec.

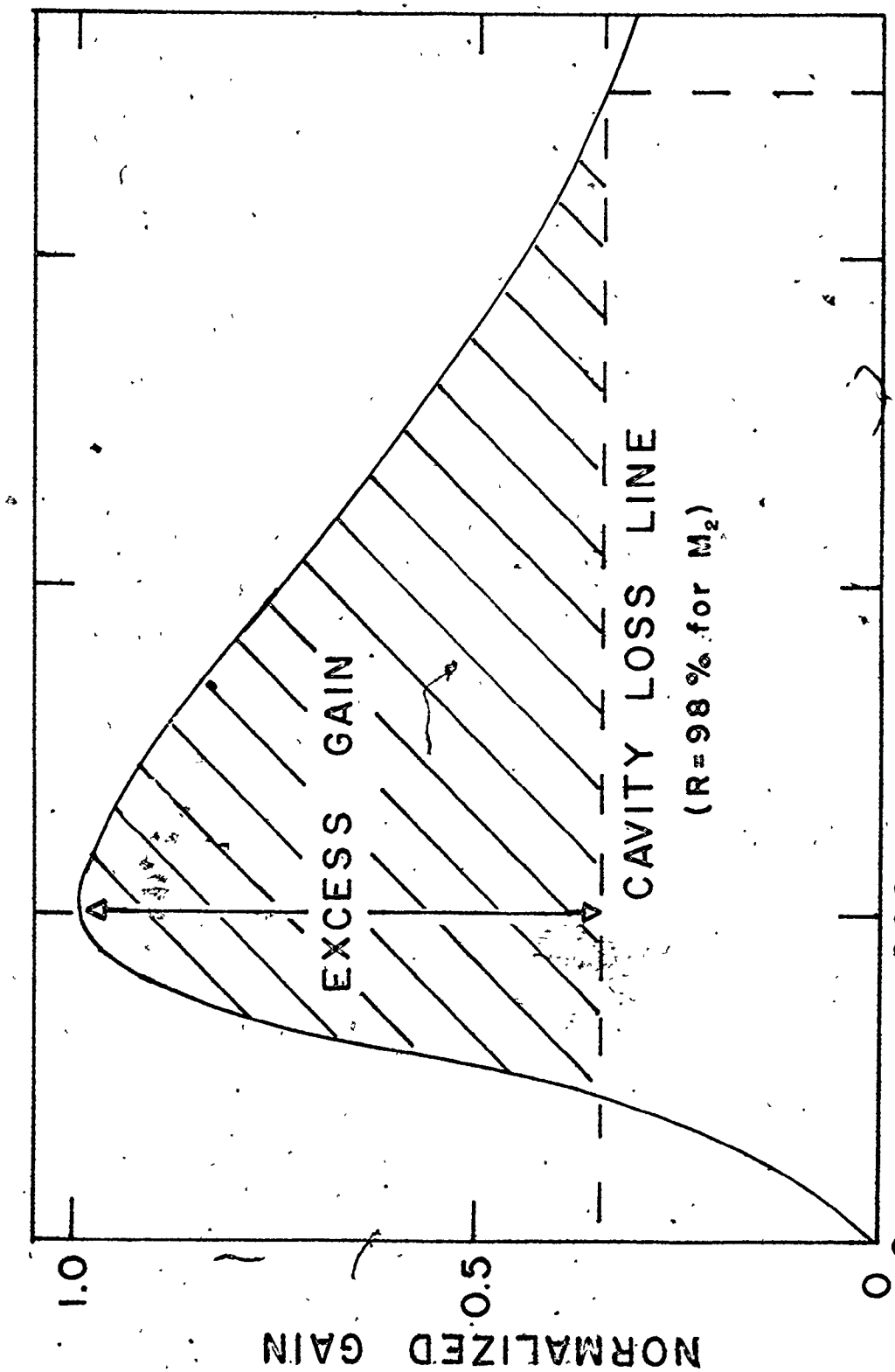
NORMALIZED GAIN
1.0
0.5
0
200
400
600
TIME (ns)
EXCESS GAIN
CAVITY LOSS LINE
(R=98 % for M2)

gain (G) normalized to the peak gain (G_o) used for the 12.08 μm laser. The area above the threshold line corresponds to the amplification required to create an in-cavity power of .1W. The risetime of the gain was assumed to follow approximately the pump pulse. The other part of the gain curve was obtained from measurements of the time delay between the beginning of the pump pulse and MIR pulse, for a variety of cavity losses. The time delays approximately indicate where the gain is equal to the cavity loss. In Fig. 19, a time delay of 700 nsec was observed when a gold mirror (M_2 see Fig. 8) was placed at one end of the MIR cavity. Because the minimum area above threshold is constant and the time delays are known experimentally for different threshold lines, the gain curve was obtained by treating these data in a self-consistent manner. The accuracy of the excess gain estimate is hence obviously limited by an accurate knowledge of the time delays and cavity loss lines, but depends only slightly on the amplification factor.

An identical procedure was employed for the R(16) pumped line. However, the excess gain corrections were larger than for the R(30) case, caused by shorter time delays observed at low cavity losses.

REFERENCES

1. T.Y. Chang and T.J. Bridges, Opt. Commun. 1, 423 (1970).
2. M. Rosenbluh, R.J. Temkin and K.J. Button, Appl. Opt. 15, 2635 (1976).
3. J.J. Gallagher, M.D. Blue, B. Bean and S. Perkowitz, Infrared Phys. 17, 43 (1977).
4. T.Y. Chang and J.D. McGee, Appl. Phys. Lett. 28, 526 (1976).
5. N.V. Karlov, Appl. Opt. 13, 301 (1974).
6. J.P. Aldridge III, J.H. Birely, C.D. Cantrell III, D.C. Cartwright, "Experimental and Theoretical Studies of Laser Isotope Separation", in Physics of Quantum Electronics Vol. 4 (1976) page 57.
7. T.Y. Chang and J.D. McGee, Appl. Phys. Lett. 29, 725 (1976).
8. D. Seligson, M. Ducloy, J.R.R. Leite, A. Sanchez and M.S. Feld, IEEE J. Quantum Electron. QE-13, 468 (1977).
9. F.W. Taylor, J. Quant. Spectrosc. Radiat. Transfer 13, 1181 (1973).
10. S. Urban, V. Spirko, D. Papousek, R.S. McDowell, N.G. Nereson, S.P. Belov, L.I. Gershtein, A.V. Maslovskij, A.F. Krupnov, J. Curtis and K. Rao, J. Mol. Spectrosc. 79, 455 (1980).
11. Chinh Dang of McMaster University, private communication.

12. A.L. Schawlow and T.A. Townes, "Microwave Spectroscopy", McGraw Hill, New York, 1955.

13. G. Herzberg, "Infrared and Raman Spectra", Van Nostrand Co., Princeton, 1945.

14. K. Gullberg, B.Hartmann and B. Kleman, Phys. Scripta 8, 177 (1973).

15. L.E.S. Mathias, A. Crocker and M.S. Wills, Phys. Letters 14, 33 (1965).

16. F. Shimizu, J. Chem. Phys. 52, 3572 (1970).

17. J.R. Tucker, Proc. Int. Conf. Submillimeter Waves and Their Applications (Atlanta, Ga. 1974).

18. R.J. Temkin and D.R. Cohn, Opt. Commun. 16, 213 (1976).

19. J.R.R. Leite, R.L. Sheffield, M. Ducloy, R.D. Sharma and M.S. Feld, Phys. Rev. A 14, 1151 (1976).

20. R.L. Panock and R.J. Temkin, IEEE J. Quantum Electron. QE-13, 425 (1977).

21. H.J.A. Bluyssen, R.E. McIntosh, A.F. van Ettegen and P. Wyder, IEEE J. Quantum Electron. QE-11, 341 (1975).

22. J. Heppner, C.O. Weiss, U. Hübner and G. Schinn, IEEE J. Quantum Electron. QE-16, 392 (1980).

23. M. Sargent III, M.O. Scully and W.E. Lamb Jr., "Laser Physics", Addison-Wesley, Massachusetts, 1974.

24. A. Yariv, "Quantum Electronics", Second edition, John Wiley and Sons, New York, 1975.

25. T.A. DeTemple, "Infrared and Millimeter Waves", Vol. I, ed. K.J. Button, Academic Press, p. 129 (1979).

26. Z. Drozdowicz, R.J. Temkin and B. Lax, IEEE J. Quantum Electron. QE-15, 170 (1979).

27. S.M. Hamadani, N.A. Kurnit and A. Javan, Chem. Phys. Letters 49, 277 (1977).

28. A.J. Beaulieu, Appl. Phys. Lett. 16, 504 (1970).

29. R. Fortin, M. Gravel and R. Tremblay, Can. J. Phys. 49, 1783 (1971).

30. J. Reid, "TE CO_2 laser dynamics", Ph.D. thesis, McMaster University, 1974.

31. F.A. Al-Watban, R.G. Harrison, J.G. Crowder and C.R. Pidgeon, J. Phys. D: Appl. Phys. 10, L167 (1977).

32. C.R. Jones, M. I. Buchwald, M. Gundersen and A.H. Bushnell, Opt. Commun. 24, 27 (1978).

33. T. Yoshida, N. Yamabayashi, K. Miyazaki and K. Fujisawa, Opt. Commun. 26, 410 (1978).

34. A. Scalabrin and K.M. Evenson, Opt. Lett. 4, 277 (1979).

35. M. Wahlen, R.S. Eng and K.W. Nill, Appl. Opt. 16, 2350 (1977).

36. E. Arié, N. Lacome and C. Rossetti, Can. J. Phys. 50, 1800 (1972).

37. V.N. Faddeyeva and N.M. Terent'ev, "Tables of the Probability Integral for Complex Argument", Pergamon Press, 1961.

38. K. Shimoda, Y. Ueda, J. Iwahori, Appl. Phys. 21, 181 (1980).

39. K.J. Siemsen and J. Reid, Appl. Opt. 17, 3523 (1978).

40. E.J. Danielewicz, E.G. Malk and P.D. Coleman, Appl. Phys. Lett. 29, 557 (1976).

41. B. Walker, G.W. Chantry and D.G. Moss, Opt. Commun. 23, 8 (1977).

42. T.Y. Chang, T.J. Bridges and E.G. Burkhadt, Appl. Phys. Lett. 17, 357 (1970).

43. T.A. Znotins, J. Reid, B.K. Garside and E.A. Ballik, to be published, Opt. Lett. December (1980).